Diploma thesis

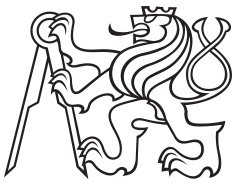

Czech Technical University in Prague

F4

Faculty of Nuclear Sciences and Physical Engineering
Department of physics

Statistical analysis of measurements of fusion neutrons and photo-neutrons at the COMPASS tokamak

Bc. Lukáš Lobko

Supervisor: Ing. Ondřej Ficker
April 2022

ČESKÉ VYSOKÉ UČENÍ TECHNICKÉ V PRAZE
FAKULTA JADERNÁ A FYZIKÁLNĚ INŽENÝRSKÁ
PRAHA 1 - STARÉ MĚSTO, BŘEHOVÁ 7 - PSČ 115 19

Katedra: fyziky *Akademický rok:* 2020/2021

ZADÁNÍ DIPLOMOVÉ PRÁCE

Student: Bc. Lukáš Lobko

Studijní program: Aplikace přírodních věd

Obor: Fyzika a technika termojaderné fúze

Název práce: (česky) Statistická analýza měření fúzních neutronů a fotoneutronů na tokamaku COMPASS

Název práce: (anglicky) Statistical analysis of measurements of fusion neutrons and photo-neutrons at the COMPASS tokamak

Pokyny pro vypracování:

1. Analýza a diskriminace píků odpovídajících neutronům a fotonům tvrdého rentgenového záření z měření při speciálních kampaních na tokamaku COMPASS
2. Statistická analýza neutronových signálů za celou historii tokamaku COMPASS
3. Objasnění hlavních trendů v datech na základě parametrů plazmatu a technických parametrů
4. Srovnání s relevantními modely
5. Důsledky pro neutronovou diagnostiku navrhovaného tokamaku COMPASS-U

Doporučená literatura:

[1] M. F. L'Annunziata: Handbook of Radioactivity Analysis, 3rd Ed., Elsevier, 2012

[2] H. W. Hendel, D. L. Jassby: Tokamak as a Neutron Source, Nucl. Sc, Eng. 106, 2 (1990)

[3] Y. Wu: Fusion Neutronics, Springer Nature Singapore, 2017

[4] I. Hutchinson: Principles of Plasma Diagnostics, 2nd Ed. Cambridge U. Press, 2002

[5] G. Tardini et al.: First neutron spectrometry measurements in the ASDEX Upgrade tokamak, Jinst 7 C03004 (2012)

[6] H. W. Hendel et al.: Fusion-neutron production in the TFTR with Deuterium neutral-beam injection, Journal of Fusion Energy 5, 231-244 (1986)

[7] O. N. Jarvis et al.: Photoneutron production accompanying plasma disruptions in JET, Nuclear Fusion 28, 11 (1988)

Jméno a pracoviště vedoucího diplomové práce: Ing. Ondřej Ficker

Ústav fyziky plazmatu AV ČR, Za Slovankou 1782/3, 182 00 Praha 8
FJFI ČVUT v Praze, Břehová 78/7, 115 19 Praha 1

Datum zadání diplomové práce: 23.10.2020

Termín odevzdání diplomové práce: 03.05.2021

Doba platnosti zadání je dva roky od data zadání.

……
garant oboru

…….. ……..
vedoucí katedry *děkan*

V Praze dne 23.10.2020

Acknowledgements

Many thanks to my supervisor Ing. Ondřej Ficker for guiding my diploma thesis, for his important advices and comments.

Declaration

I declare that I have prepared the submitted work independently and that I have listed all the used literature.

In Prague, 27. April 2022

Abstract

This diploma thesis presents an extensive statistical analysis of all fusion neutron and photo-neutron measurements performed during a long operational period of the COMPASS tokamak. Measured data reveal main trends and correlations of neutron and photo-neutron yield with the various tokamak technical parameters and plasma behaviour. The results contribute to the fusion power research area and to the problematics of runaway electrons in the tokamak plasma as well.

Keywords: neutron, photo-neutron, neutron/γ discrimination, wall shielding, absorbed dose of radiation, runaway electrons, COMPASS, neutron detectors, NBI plasma heating, H-mode, argon, photo-disintegration

Supervisor: Ing. Ondřej Ficker
IPP of the Czech Academy of Sciences,
Za Slovankou 1782/3,
Prague 8

Abstrakt

Tato diplomová práce prezentuje rozsáhlou statistickou analýzu fúzních neutronů a foto-neutronů ze všech měření provedených za dlouhou provozní dobu tokamaku COMPASS. Naměřená data odhalují hlavní trendy a korelace neutronových a foto-neutronových výtěžků s různými technickými parametry tokamaku a s chováním plazmatu. Výsledky přispívají do oblasti výzkumu fúzního výkonu stejně jako k problematice ubíhajících elektronů v tokamakovém plazmatu.

Klíčová slova: neutron, foto-neutron, neutron/γ diskriminace, stínění, absorbovaná dávka záření, ubíhající elektrony, COMPASS, neutronové detektory, NBI ohřev plazmatu, H-mód, argon, foto-disintegrace

Překlad názvu: Statistická analýza měření fúzních neutronů a foto-neutronů na tokamaku COMPASS

Contents

Figures

Tables

Introduction

Research in the area of thermonuclear fusion is gaining in importance with each passing year. With the completion of the forthcoming thermonuclear reactor ITER in France, thermonuclear fusion is enjoying increasing interest in media. In a few decades the energy from thermonuclear reactors should help significantly with the problems connected with the global warming phenomenon and closing coal and even fission nuclear power plants, although there is yet no way, how to replace them effectively given the still growing world energy consumption.

With increasing size and with higher power of the auxiliary plasma heating of the new tokamaks like ITER, COMPASS-U, the fusion power mediated by fusion neutrons rapidly increases. Thus neutron diagnostics is gaining in importance. At the ITER tokamak, an extensive neutron diagnostic set will be installed for the monitoring of the fusion power.

Existing neutron diagnostics on the tokamaks consists of a few types of detectors like proportional counters, fission chambers, activation foils. Especially the scintillation detectors are very often an important part of a neutron diagnostics at the tokamaks. Neutron detectors on small devices are often operated outside the single event counting regime and give only relative information on the neutron fluxes.

At the COMPASS tokamak, a neutron diagnostics consists of the scintillation detector EJ410 operated in a specific current regime with high impedance, two 3He neutron counters and a pair of scintillation detectors NuDET used for specific measurements. All detectors have a temporal resolution.

This diploma thesis is divided into two parts. In the first part, we will present a statistical analysis of all fusion neutron signals from all neutron detectors during the whole tokamak COMPASS standard operational period (2013-2020). The tokamak COMPASS started its operation a few years earlier, but a neutron diagnostics started to measure first signals in 2013.

In this analysis, we will reveal the main trends in the data and present the most significant correlations of fusion neutron yield with tokamak technical parameters and plasma behaviour. There is also demonstrated a very specific measurement of the neutron attenuation coefficient of the main shielding wall around the COMPASS tokamak. A brief theoretical background of physical and technical phenomena used in the analysis along with more detailed description of all neutron detectors at the COMPASS tokamak is presented as well.

The second part is focused on the measurements of photo-neutrons, which are presented due to collisions of runaway electrons with the plasma facing components. A statistical analysis of all runaway campaigns is presented and the most significant correlations with the tokamak technical parameters and plasma behaviour are revealed. There is also demonstrated a technique of neutron/HXR peak discrimination in NuDET scintillation detector. In the last chapter, an estimate of RE energies is described, based on photo-neutron measurements. A brief theoretical background of used physical phenomena is presented as well to help the reader in better understanding the text.

Part I

Measurement of fusion neutrons at the COMPASS tokamak

Chapter 1

Brief theoretical background

1.1 Neutrons in thermonuclear fusion

Currently, the research of thermonuclear fusion as a way to a source of clean energy is working almost exclusively with nuclear fusion reaction deuterium-deuterium (DD) at most tokamaks and gradually also with deuterium-tritium (DT) fusion reaction like at JET and coming ITER tokamak. The reason is a very simple, as these reactions are by far the most "easily accessible" from all set of various exothermic thermonuclear reactions.

The term "easily accessible" is in quotes, because it is not easy at all. For example, taking parameters of ITER tokamak, that should produce ten times more fusion power than the required heating power, here the plasma with density approx. 1e20 m^{-3} of a volume 840 m^3 will have a temperature approx 150 million °C (i.e. 13 keV). Systems, that will generate and hold this configuration are extremely technologically complex and in many ways completely unique in the world. [7]

At the COMPASS tokamak, the fuel is a deuterium gas, thus the very most of the released and detected neutrons are from DD nuclear reaction. Anyway, naturally the DT neutrons are not completely ruled out, because of generating tritium from DD fusion reaction:

$$\mathrm{D} + \mathrm{D} = {}^{3}\mathrm{He} + \mathrm{n} \tag{1.1}$$

$$\mathrm{D} + \mathrm{D} = \mathrm{T} + \mathrm{p} \tag{1.2}$$

Both possible branches have almost the same cross-section. Actual state of neutron diagnostics at COMPASS tokamak does not allow proper measurement of neutron energy spectra, so to distinguish between DD neutrons of

energy 2.5 MeV energy and DT neutrons of energy 14.1 MeV (if they are present in detectable amount) is currently not possible. Design and utilisation of proper neutron energy spectra diagnostics is very complicated and it probably will not pay off in tokamaks of small sizes like COMPASS. [8]

1.2 Plasma heating system

1.2.1 Ohmic heating

Sufficient plasma heating is a key aspect to raise fusion processes in plasma, from which neutrons come. Basic plasma heating is done by Ohmic (or Joule) heating generated by the passing electric current through the plasma. This kind of plasma heating can usually heat the plasma to about 1 keV. But optimal plasma temperature for DT fusion is somewhere in the range of 10-20 keV (ITER should reach to approx. 13 keV).

There are more reasons, why we can not just rise the plasma current for more Ohmic heating. For example, Ohmic heating becomes less and less effective due to decreasing plasma resistance with temperature rising, or the high plasma current I_p leads to to much intensive magnetic poloidal field and thus "kink" and other MHD instabilities begin to occur. So today, I_p is chosen so to optimize the confinement of plasma energy more than to reach maximum heating possibilities. Also, it is very practical to have some external (independent on plasma) heating source, not affecting plasma confinement configuration by itself like Ohmic heating. In practice, two methods for external heating source are used - radiofrequency heating and NBI heating. [9]

1.2.2 Radiofrequency heating

The principle of radiofrequency heating is quite simple. The generator produces electromagnetic waves, which are led through the transmission lines to the antenna, which sends the electromagnetic waves of specific frequency to the plasma, where the wave transmits its energy to plasma particles. Those specific frequencies are ion and electron cyclotron frequencies, on which the resonance with plasma particles occurs. The used frequencies also depend on plasma configuration, mainly on the value of toroidal magnetic field.

For ion cyclotron resonance heating, frequencies are tens of MHz in the

order of magnitude. The main disadvantage is, that these frequencies can not travel through vacuum and thus the antenna must be basically in "contact range" with plasma. This fact can naturally lead to release of impurities to plasma and so to rise of radiation losses of plasma energy.

Electron cyclotron resonance heating uses much higher frequencies, even in order of low hundreds of GHz. The advantage is, that these frequencies can be well transferred by metal or other waveguides, so the antenna does not have to be in contact of plasma. Also, this type of heating can be more specifically focused to a local place in plasma, helping with various instabilities mitigation. [7]

1.2.3 NBI heating

The second way of external plasma heating is by using NBI (Neutral Beam Injection) heating. The principle is as follows and also shown in figure 1.1. Firstly, the ions are generated in an ion source, e.g. by using RF antenna. Then, ions are accelerated through a grid by electric potential and making the beam of ions with necessary energy of each charged particle. Than, the ions need to be neutralised (charged particles can not reach plasma due to magnetic field). This is typically done by directing the beam through neutral gas in order to impose charge-exchange between fast ions and neutral particles of the gas. Non-neutralized fast particles are deflected to dumps. The result is a beam of neutral particles with high energy.

Energy of particles injected to plasma is chosen so the particles can penetrate to the core of the plasma, before they are ionized. So the required energy of the particles depends on the plasma size, density and its value is from tens of keV as at the small COMPASS tokamak to units of MeV as in a large device like ITER tokamak. At these high particle energies the neutralization process in NBI machine is inefficient, so the ion source typically produces negatively charged ions of deuterium. An added electron is weakly bound and so the charge-exchange process with neutral gas is much more effective. [1, 10]

1.2.4 COMPASS tokamak - NBI heating system

One of the biggest upgrades of tokamak COMPASS in correlation to its previous version COMPASS-D in Culham in the UK was adding new NBI heating system. It consists of two identical NBIs. Both of them produce deuterium atoms with energy of 40 keV creating a beam (before neutralization) in range of approx. 6 - 12 A. NBI beams can last up to approx. 300 ms

each, most often approx. 100 ms. Thus they can supply more than 100 kJ of energy to the plasma.

It is good to mention here, that not all NBI beam particles have required 40 keV energy. In reality, there is a significant part of particles with half the energy, i.e. 20 keV, third the energy and tenth the energy. It is due to processes of ionization of deuterium gas in the ion source. Here the ionized molecules of D_2, D_3 and D_2O arise, too. With lower energies, these neutralized particles will not reach the core, but only the edge of plasma and thus their energy is not properly used to heat the plasma.

The position of NBIs was variable at COMPASS. They could both inject the beams tangentially co-current for maximize the heating ability, or they could be injected in mutually different directions for non-rotating plasma. [1, 11, 12]

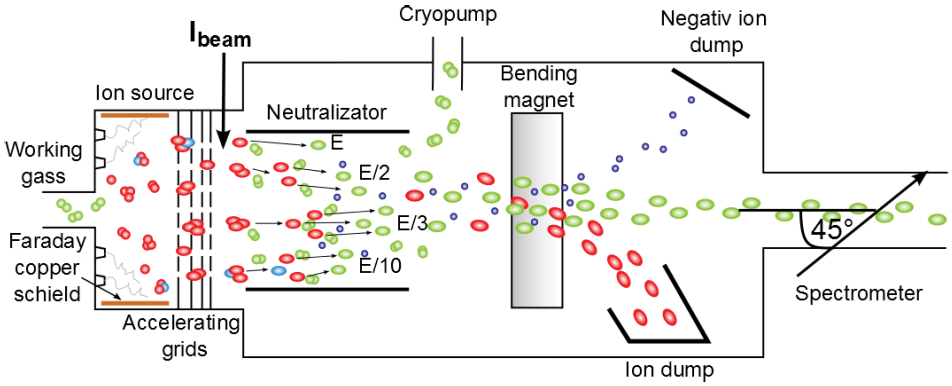

Figure 1.1: Scheme of NBI principle. [1]

1.3 H-mode

In the general fusion theory, one of the basic requirements to make a progress towards practically manageable fusion is to construct a tokamak with the highest possible combination of parameters n_p, T_p and τ_E (plasma density, plasma temperature and plasma energy confinement time), which follows from "triple product" rule. Making a significant improvement of these parameters without a significant upgrade of a tokamak machine itself was a quite hard in earlier times. Then, so-called H-mode (high confinement) regime of plasma confinement was reached. It was observed firstly at ASDEX tokamak in Germany at 1981 (original paper from 1982 [13]).

The main distinguishing feature of H-mode is a formation of a large density gradient region at the edge of plasma (SOL), as we can see in the figure 1.2. This pedestal creates a natural plasma transport barrier, which leads to roughly two-times higher plasma energy confinement time τ_E, which was at

the time of the discovery a very significant improvement. It also improves a T_p as well. H-mode regime and its advanced modes are expected at ITER tokamak. [2, 9, 14]

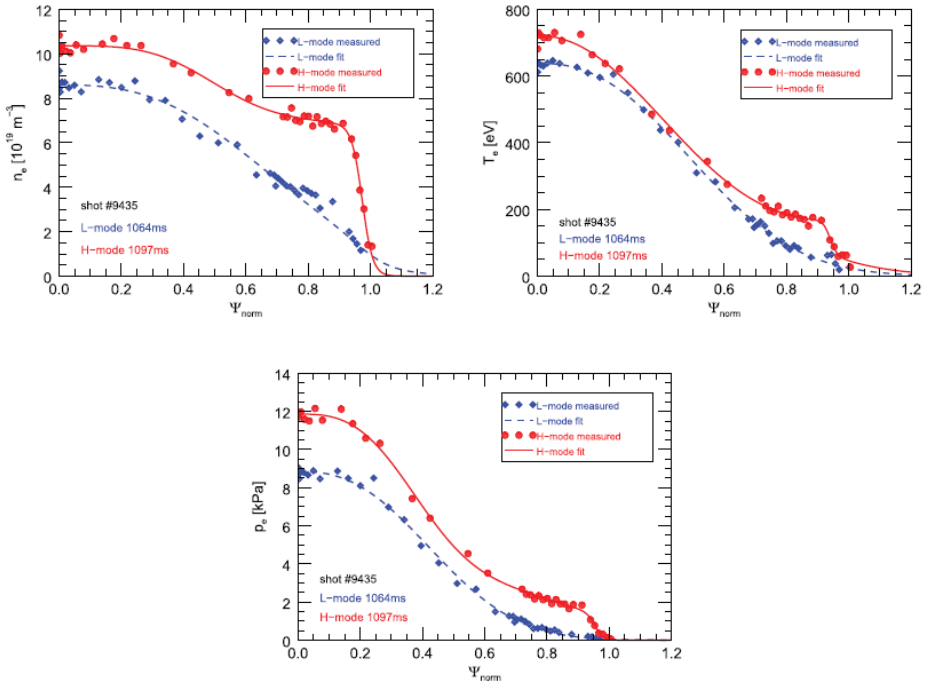

Figure 1.2: Radial profiles of density, temperature and pressure in H-mode. [2]

1.3.1 ELMy H-mode

As a proposed regime at ITER tokamak, H-mode was and still is intensively studied. To reach a H-mode, it was observed, that total power over separatrix (affected by energy gains like Ohmic, radiofrequency or NBI heating power and losses like radiation) needs to trigger specific value. This H-mode threshold depends mainly on plasma density n_p, toroidal magnetic field B_T and plasma volume (or better plasma surface). [15]

As it is quite usual, different plasma configurations are accompanied with various instabilities. It is the same in the case of H-mode plasma. The usual result of the presence of specific instabilities (without going into details) is so-called Edge Localised Modes H-mode, shortly ELMy H-mode. This mode is manifested by the recurrent ejections of plasma filaments from the plasma edge. This phenomena has both positive and negative effects. One of the problems is, that these ejected plasma blobs can possibly damage plasma facing components like divertor or the first wall. On the other hand, at the plasma edge the impurities are often gathered, so these plasma blobs from

the edge lead to better impurities removal and thus to better plasma purity and lower radiation losses. The theory distinguishes at least between 3 ELMy H-mode types.

Type I ELMy H-mode is recognized by the fact that increase of heating power leads to increase of ELM frequency. Type I ELMs are observed, when power is well above the H-mode threshold. The H-mode and ELMs are mostly visible at H_α radiation diagnostics, like in the figure 1.3. A sudden drop of H_α radiation can be clearly seen in both presented discharges around 1070 ms - this phenomena is called the L-H transition. After that, we can see distinguishable peaks, each of them corresponds to an ELM event (plasma blob ejection). Type I ELMs are characterized with low frequency and high amplitude. The ELMs in the figure are most probably type I ELMs. Generally speaking, type I ELMs lead to more evident increase of confinement time and to higher stored plasma energy and density.

Type III ELMy H-mode has usually much higher ELM frequency but much lower amplitude. It usually occurs, when power is just above the H-mode threshold. this ELM type is thus naturally safer for plasma facing components, as the plasma blobs are much smaller. The main characteristic feature is that power rise leads to decreasing of the ELM frequency in contrast of type I ELMs.

Type II ELMy H-mode (also "grassy" term is used) is quite rare, because it occurs only with strongly shaped plasma configurations. This type was not observed at the COMPASS tokamak. Generally speaking, there is naturally much less information about this type. [16]

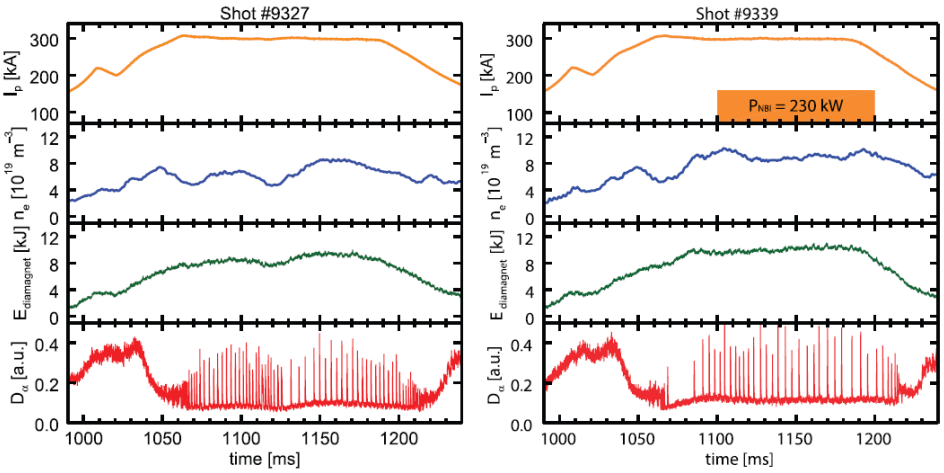

Figure 1.3: Examples of ELMy H-modes. [2]

1.4 Absorbed dose and equivalent dose

In the chapter 4, a rough estimate of a COMPASS and COMPASS-U wall shielding efficiency will be presented. For the calculation of the radiation impact on the living tissue the quantity named absorbed dose D must be first determined. D indicates, how much energy was absorbed in 1 kilogram of the given material (body, tissue, organ, ...). The unit is Gray (Gy). It is obvious, that 1 Gy = 1 $\frac{\mathrm{J}}{\mathrm{kg}}$.

However, the true biological impact doesn't just matter only on the amount of absorbed energy, but it depends on the kind of the radiation, too. For this purpose another quantity named equivalent dose H was introduced like

$$H = W_R \cdot D, \tag{1.3}$$

where W_R is the „radiation weighting factor". W_R is dimensionless quantity and the default value is $W_R = 1$ for the HXR/γ radiation. The factor is larger for some other types of radiation. For example $W_R = 10$ for neutrons with energies between (10 keV - 100 keV). This means, that these neutrons are ten times more dangerous for living tissue than HXR/γ radiation, when the same dose is absorbed. The unit of H is Sievert (Sv). Sievert is mathematically the same unit as Gray, but the difference in the meaning is obvious. For more details see [17].

Chapter 2

COMPASS neutron detectors

The first recorded discharge of the COMPASS tokamak took place in August 2008 and since then the COMPASS generated more than 21 000 discharges with various plasma setup and machine technical parameters. Measurement of neutrons at the COMPASS tokamak started almost 5 years later, in February 2013 - by the discharge discharge #4508, in which the scintillation detector EJ410 measured for the first time.

3-Helium filled detectors Chadwick and Oliphant began to detect neutrons in August 2016 - discharge #12308. Finally, since 2017 two NuDET detectors were available for various specific measurements like RE campaigns discussed in the part II.

Measurement of neutron fluxes at the COMPASS tokamak belongs rather to a category of secondary, supporting diagnostics. One of the reasons is, that COMPASS is a small tokamak. It is naturally true, that the bigger and thus much more "powerful" the fusion reactor is, the neutron diagnostics rapidly grows in importance.

2.1 EJ-410 detector

Signals of scintillation neutron detector EJ-410 serve here at COMPASS tokamak as the default values for the first look at neutron presence in a discharge. The detector, however, does not measure specific neutrons, but a more complex, summed signal, figure 2.2. Signal is proportional primarily to flux of the neutrons but also affect by their energies. The character of the signal is given by the high impedance of 1 kΩ at data acquisition

system. Integrals of the signals serve well for mutual comparisons of the discharges, where the fusion power was higher or lower, but the information about absolute values like total neutron yield from the tokamak, absolute value of neutron flux etc., can not be obtained without detailed modelling of neutron transport through tokamak components and absolute calibration of the detector.

Like almost all scintillation detectors, detector EJ-410 is also more or less sensitive to HXR radiation. Thus, mainly in the cases, when the disruption occurs in the discharge, where usually HXR radiation is generated by runaway electrons, signal needs to be properly filtered (if it is possible) before using the signal as neutron detector. On the other hand, this HXR sensitivity can be useful in RE campaigns. On the other hand, it makes the photo-neutron detection much more complicated in the HXR background.. This theme will be further discussed and analysed in the part II.

Detector is compoused from acrylic disc (neutron-proton backscattering) with ZnS(Ag) (scintillation material) and PMT. For more technical info about detector EJ-410, see [18].

2.2 3He detectors

At the COMPASS tokamak, two 3He gas filled detectors with working names Chadwick and Oliphant are in operation. Unlike the EJ410 they are not used for quick discharge comparison, but they provide number of neutron counts, because they are used together with neutron counters (Neutrons Pulse Monitor - NPM). Thus, these detectors record the amplitude and the time of arrival of a single detected particle, one by one. So, the number of measured records is the number of measured neutrons. In the figure 2.2, every dot represents a record of a single detected particle.

The amplitude of each measured particle can be weakly proportional to its energy, but the relation seems to be insufficient to derive neutron energy spectra. Exothermic reaction of 3He(n,p)T releases a lot kinetic energy (about 700 keV), thus making energy spectra calculations quite unreliable. Furthermore the cross-section of the reaction is quickly changing with the incident neutron energy and a fraction of the energy of the products can be lost.

A disadvantage is the dead time of neutron counter, but the sensitivity of the detector is such that the dead time does not play a significant role during most of the COMPASS discharges. At the COMPASS-U, where much higher neutron fluxes are expected, it could be a problem.

Big advantage of these detectors is, that they are almost insensitive to HXR radiation. This means, that for example unexpected disruption and thus a raised cluster of HXRs mostly does not affect the measurement in

contrast of scintillation detectors like EJ-410. This property is even more evident in photo-neutrons detection during RE campaigns, as it will be more discussed in part II.

Detector Oliphant has also HDPE cylinder around itself for the higher detection efficiency in contrast to Chadwick, which is usually surrounded by lead shielding. For more technical info about 3He detectors Chadwick and Oliphant, see [18].

2.3 NuDET detectors

Two neutron scintillation detectors NuDET are used at the COMPASS tokamak for various specific measurements. For example, in the chapter 4 use of these detectors for measurement neutron fluxes behind the main shielding wall around the COMPASS tokamak will be presented.

Signal of the NuDET detector measures voltage continuously in time, fig. 2.2. Every detected particle creates voltage peak, where the amplitude of the peak is in a part proportional to its energy. In a part, because technical parameters of the detector leads to unreliable particles energy calculations, like energy overflow in detecting reaction 6Li(n,α)T.

These detectors are characterised, among other things due to a very small thickness of the scintillation layer, by a huge difference between the neutron and HXR peaks and thus the discrimination from each other can be done in the cases, where neutron or HXR fluxes are not too high, thus without pile-ups. This property is very useful in the part II during RE campaign measurement. For proper individual peaks measurement low impedance of 50 Ohm at data acquisition system and at least 50 MHz sampling rate are necessary to reliably catch HXR peaks.

The core of the detector is composed of the small scintillation crystal ZnS(Ag) in the shape of a thin cylinder with thickness 4 mm and diameter 40 mm. Scintillation crystal is connected to a PMT. On the detection area of the crystal a thin layer of ^{6}LiF is applied. This layer converts neutrons to the charged particles through the nuclear reaction

$$\mathrm{n} + {}^6\mathrm{Li} \rightarrow \alpha + \mathrm{T}. \tag{2.1}$$

The cross-section σ of this reaction varies in a wide range, from 1000 barn to less than 1 barn, fig. 2.1.

In the chapter 8, very rough estimate of RE beam energy will be presented, where we have used following NuDET parameters: The NuDET sensitivity is 4.5 cps/nv for thermal neutrons ($E = 0.025$ eV), declared by manufacturer. If we consider detection area of this detector (12.56 cm^2), it means, that the sensitivity for detecting thermal neutrons is 35,8 %. Every third thermal neutron, which strikes the detector, is registered.

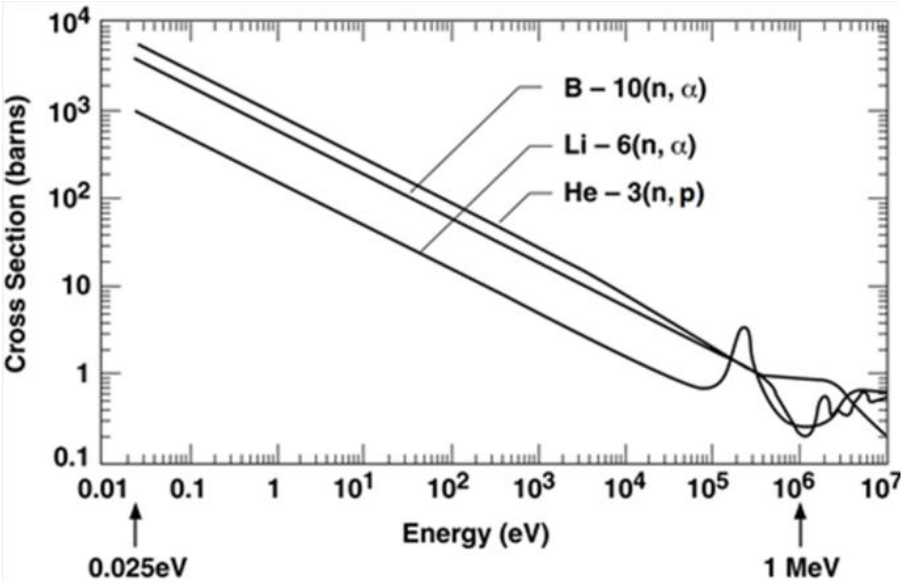

Figure 2.1: Cross section of neutron-lithium nuclear reaction, [3].

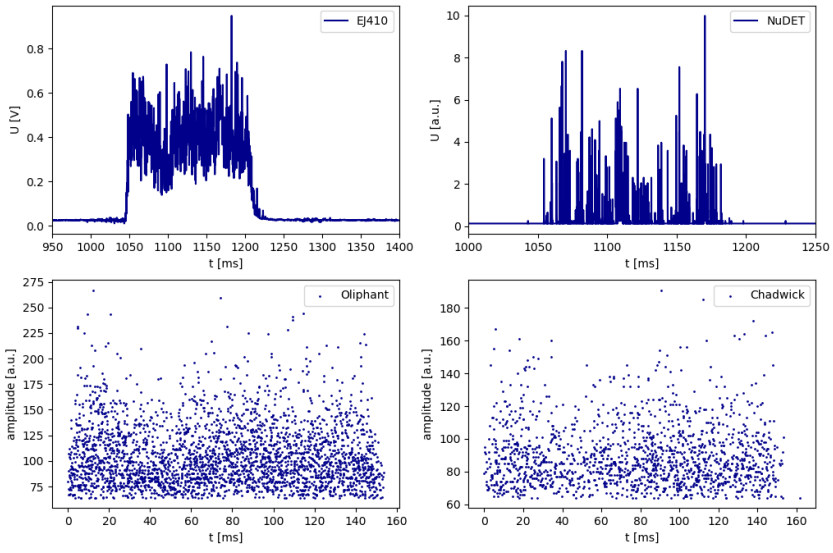

Figure 2.2: Examples of rough measured data from all neutron detectors at COMPASS tokamak from different discharges. Notice that time axis at Oliphant and Chadwick is not fitted on general discharge time axis.

Chapter 3

Statistical analysis of neutron signals during whole tokamak COMPASS standard operational period (2013-2020)

3.1 Basic overview

During the whole tokamak COMPASS operational period a lot of campaigns with various tokamak technical and plasma parameters were realised. This analysis does not include just the very last NBI campaign in July 2021. It was a very specific campaign, where the new NBI for COMPASS Upgrade with much higher heating power was tested.

Figure 3.1 displays all usable data from neutron detector EJ-410. In this stage, data are divided into two groups - RE campaigns and "the rest". This figure mainly shows, how important is to work with RE campaigns separately. Integrals of the EJ-410 signal from RE campaigns are generally much higher than in NBI and other campaigns. During the RE campaigns, the signal does not represent fusion neutrons but photo-neutrons and strong HXR radiation together. It is very different physics, so detailed study of the signals from neutron detectors from RE campaigns will be performed in the part II of this thesis.

Figure 3.2 shows all data from Oliphant detector except RE campaigns. It basically displays individual NBI campaigns or campaigns, where NBI heating system was active. The fact is that NBI power is absolutely necessary to release a detectable amount of fusion neutrons in tokamak COMPASS. This is demonstrated in figure 3.3, where a set of discharges without active NBI heating system and without RE campaigns from 3He Oliphant detector

is shown. Absolutely negligible part of this set shows non-zero values. In a detailed look at these individual discharges, it represents mainly individual disruptions with the presence of REs, so it does not represent some kind of unexpected plasma behaviour. In the next chapter, we will thus focus on smaller set of discharges, where NBI heating system is active. As will be shown below in the text, the brightest direct correlation on fusion neutrons gain is with NBI specific parameters.

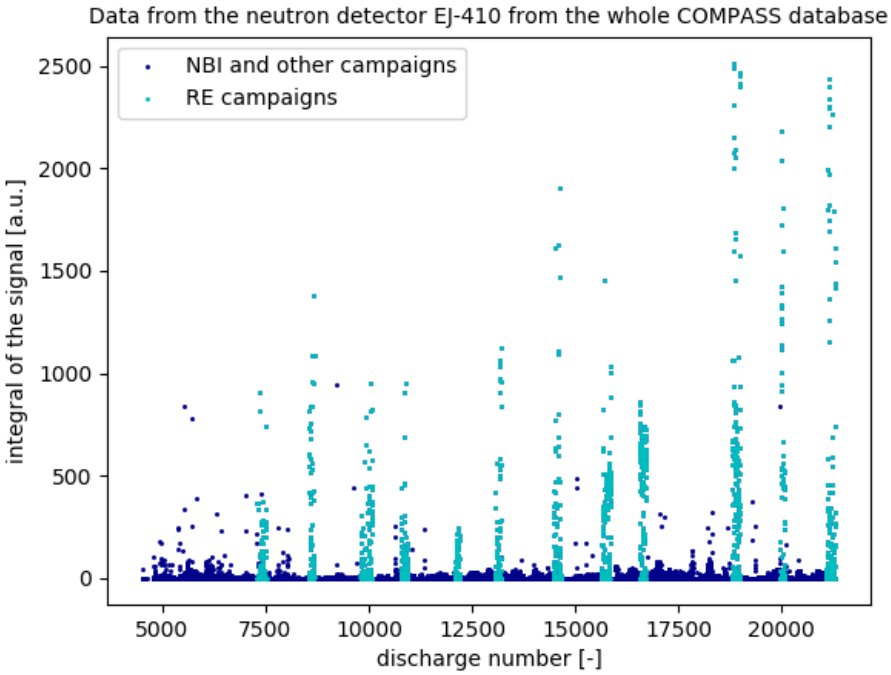

Figure 3.1: EJ-410 all data.

3.2 Filtering signals

Before the analysis itself, the set of signals from neutron detectors was properly filtered due to both physics and technical reasons. Long interval of seven years of neutron diagnostics measurements caused some changes of technical setup of detectors, for example variable value of the signal offset, PMT voltage etc. In order to properly compare the data a unified diagnostics setup is necessary.

In terms of physics, data has been filtered mainly from the three points of view. Firstly, we have focused on the discharges, where at least one of the NBI

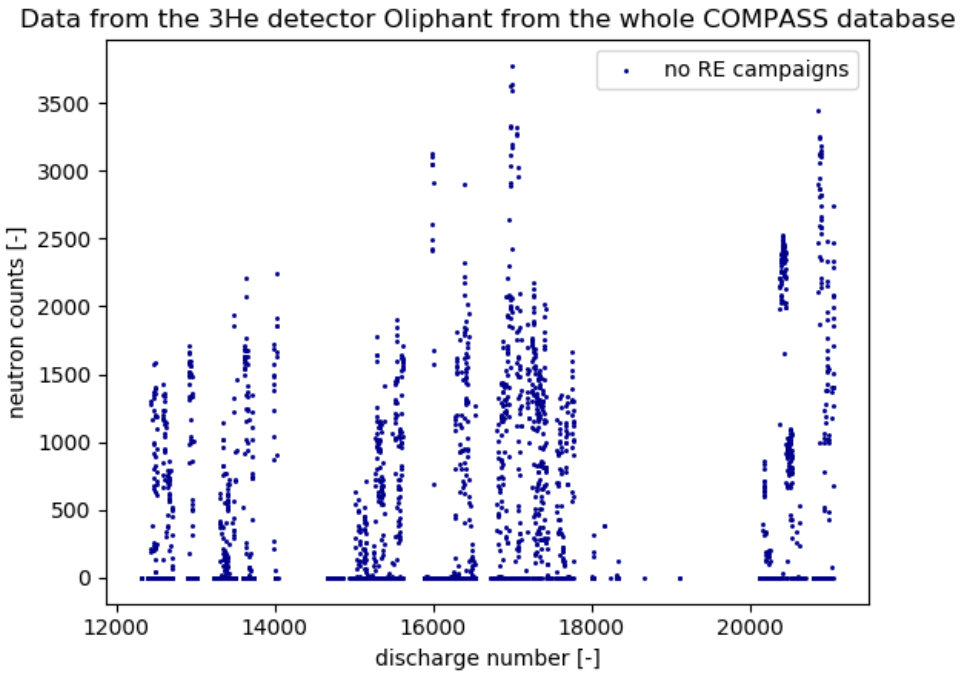

Figure 3.2: Oliphant data without RE campaigns.

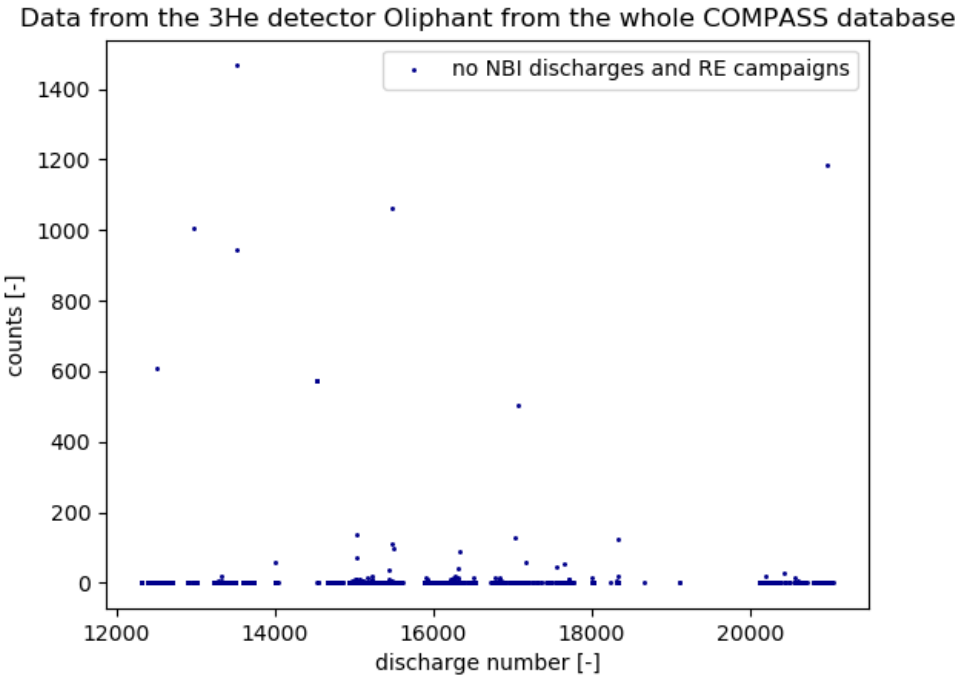

Figure 3.3: Oliphant data after filtering RE and NBI campaigns.

heating sources was operational. From the neutron signals it is clearly seen, that NBI heating source on the COMPASS tokamak is absolutely necessary for measurable amount of fusion reactions, thus for neutron generation inside the tokamak.

Secondly, discharges from runaway electron campaigns were filtered out. As was discussed in the previous chapter, in these campaigns neutrons were generated but these were not fusion neutrons but photo-neutrons. It is completely different physics, that is why analysis of RE campaigns and other campaigns are separated.

For the third time, we also do not work with all NBI discharges where a disruption has occur, only with those, where NBI operational period was fully before disruption happen. It is also clearly visible from neutron data, that without plasma existence neutrons will not arise.

Another set of more specific filters was applied in order to get a comparable data set. As a result, we have obtained a data set of approx 800 discharges from the detector EJ410, 200 signals from the Chadwick detector, 550 signals from the Oliphant detector and approx 40 signals from the NuDET detectors. Except for some isolated technical or physical anomalies, which could be all revealed only by checking every single discharge one by one (which is unrealistic in time), we have obtained data set of neutron signals, which can be properly compared and revealed main trends, correlations with various plasma parameters, etc.

For the next steps, the default values will be signals from Oliphant detector, which is, due to insensitivity to HXR radiation, more trustworthy. Also, in vast majority of discharges, where 3He detectors or NuDET detectors measured data, also EJ410 detector was in operation. Thus, EJ410 detector is mainly used for comparison and for results checking.

3.3 Neutron detectors comparison

A brief description of COMPASS neutron detectors was given in chapter 2. For neutron detection we have used three quite different detection methods. Using more different detectors is very useful for the validation of measured data. Especially in the cases, where detector measures very unexpected values, whether too low or too high, it is very useful to have available another detector for data validation.

As a one illustrative picture of, how the results of all neutron detectors are comparable, figure 3.4 presents properly filtered data sets of all detectors, especially it shows dependence of neutron yield on total injected NBI energy, as it will be discussed more in the next chapters. We can see very similar patterns by EJ410 and Oliphant. Also data from Chadwick are a quite similar, but the data set is a lot smaller and also it is very difficult to trace back,

whether the Chadwick detector was shielded or not (this is one of the reasons, why Chadwick has much smaller data set than Oliphant after the application of filters). Thus, in the subsequent analysis we are more focused on mainly Oliphant or eventually EJ410 data.

Here, in the figure 3.4, NuDET is presented with just a very small set of discharges. As was said above in Chapter 2, NuDET was used mainly on special measurements, thus we do not have many discharges to properly compare with the rest. The presented database is shown just for illustration, that there is some visible dependence on NBI energy too.

Anyway, the figure 3.4 quite clearly shows, that data from the COMPASS tokamak detectors are, generally speaking, mutually valid and trustworthy, because it is very improbable, that different detectors, with different detecting methods, with different data acquisition systems would measure the same or very similar "wrong" results.

This figure is the only one, where we can see all data sets from all neutron detectors together. The reason is, that just a direct dependence on E_{NBI} is strong enough to see some visible pattern in the whole data set. All similar figures with other plasma parameters like plasma density, electric current, magnetic field, plasma temperature, radiation loss, gas puff injection rate, plasma energy etc., do not show any signs of patterns in global view at all. This is the reason, why we will focus in the next lines on the smaller parts of our neutron data sets, where at least some plasma parameters are more or less similar and thus it is more probable of some patterns of the plasma parameters influence on neutron yield to occur.

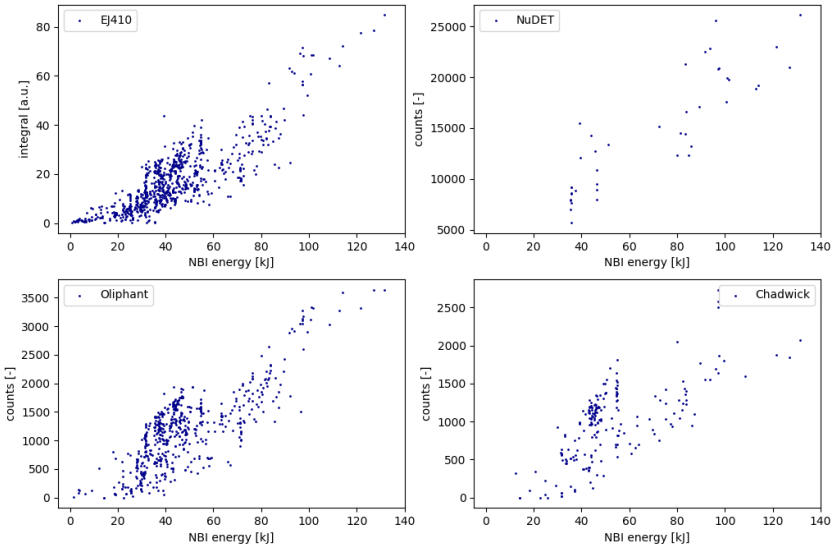

Figure 3.4: Comparison of neutron detectors at the COMPASS tokamak.

3.4 Highest neutron yield campaign at tokamak COMPASS

The NBI campaign with the highest fusion neutron yield was campaign CC19.05 - High power H-mode - scenario development (except for the very last NBI campaign, where the new NBI heating system for COMPASS-U was tested). It was in May in 2018 between discharges #16893 - #17106. Neutron yields were compared with different parameters. As was expected, the most visible direct dependency on neutron counts is on the NBI energy delivered to plasma. In this campaign, both NBIs were operational, delivered 40 keV neutral deuterium atoms. During the campaign, NBI current was changing from approx 8 to 10 A. Figure 3.5 shows dependency of neutron yield on NBI energy and as we can see, this one campaign can cover quite wide range of NBI energy. The dependence is closest to the linear function, plotted in the figure 3.5. When we realize, how complicated are processes in the plasma and thus how hard it is to see some obvious dependencies, this dependency on NBI energy is quite obvious despite the fact, that we do not compare the same plasma discharges.

The figure 3.6 complements the view on the campaign, it shows basic discharge parameters like toroidal magnetic field B_t, plasma current I_p, electron plasma density n_e and discharge duration τ. τ is presented here more like a checking parameter to complement the figure. As was expected, any hint of direct dependency on neutron yields of any of these parameters is not seen. If we focus on smaller groups of discharges, where NBI energy is very similar, the result is the same. It could be expected, that after NBI energy the next most important plasma parameters are plasma density and plasma current, because these are the two most important parameters that affect the fusion reaction rate and confinement of NBI particles. Another, in our situation, I_p can heat plasma approx. to a few hundred of eV. NBI heating on energies of 40 keV of injected particles is thus dominant next to I_p (Joule) heating. Speaking of electron plasma density n_e, the changes are moving in orders of 1e19 particles in m^{-3} and there is not observed any visible dependency on these changes in this stage of the analysis, too.

Here, it is good to mention, that we are comparing discharges, where the whole NBI energy was injected into plasma. It means, that the discharges, where the disruption occurred during the NBI injection time interval were filtered out. So the expected behaviour is, that higher I_p should lead to higher neutron fluxes, but as was already said, this behaviour was not observed. This result is probably because of a clear dominance of the influence of injected NBI energy. The influence of n_e is discussed in chapter 3.6 in detail.

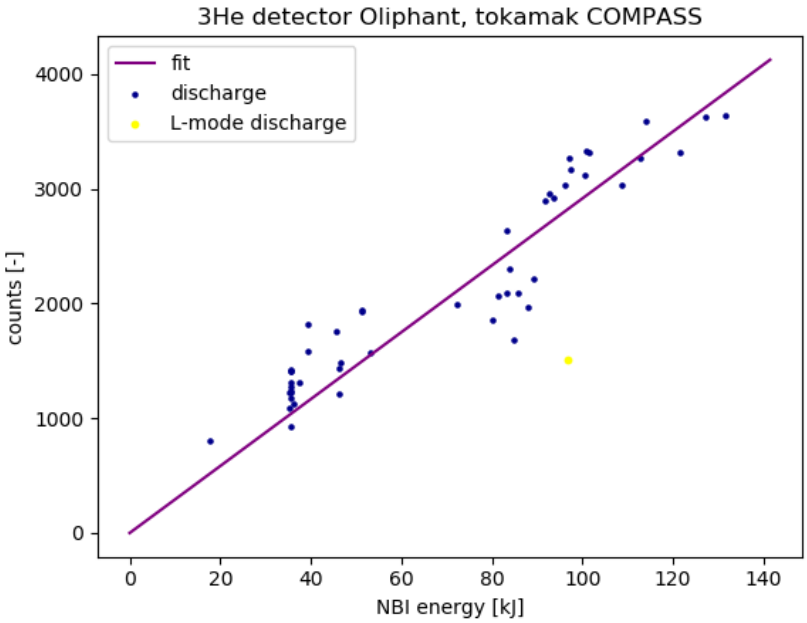

Figure 3.5: Campaign CC19.05 - High power H-mode - scenario development, Oliphant detector.

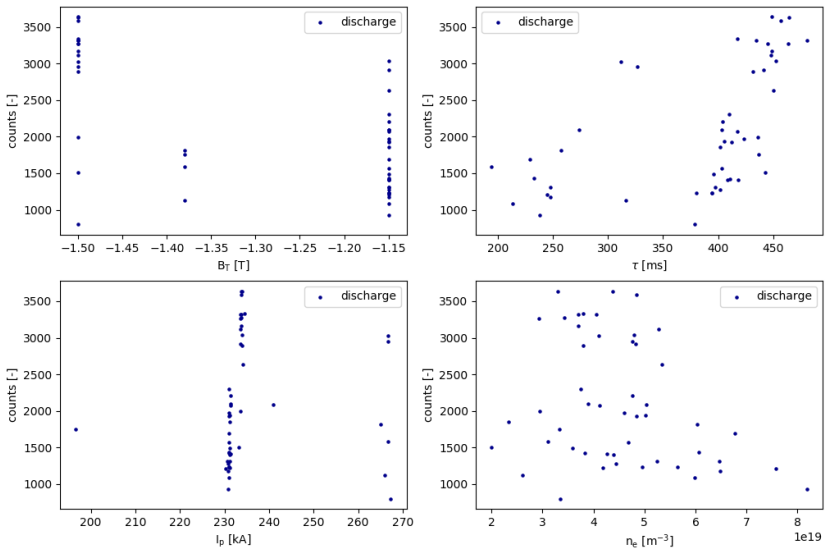

Figure 3.6: Some of basic plasma parameters - magnetic field B_T, discharge duration τ, plasma current I_p and electron plasma density n_e.

3.5 Influence of H-mode

In the next lines, we will focus our interest on a few more tokamak COMPASS campaigns, which were interesting for us from point of view of neutron yield. Note that we do not analyse a few last NBI intensive campaigns, because diagnostics of voltage on NBI2 did not measure proper values and thus we can not calculate NBI energy properly.
Back to the figure 3.5, we can see one discharge (#17050), which clearly does not fit to the "linear" trend, marked with a yellow dot. The only visible difference between this discharge and the rest is, that the plasma did not reached a H-mode of plasma confinement. In the next paragraph, we will further discuss the influence of L/H-mode on the neutron yield.

For the demonstration of the influence of "plasma mode" on the neutron yield, we made a comparison of campaigns "CC19.02 - L-mode" and previously mentioned campaign "CC19.05 - High power H-mode - scenario development". In the figure 3.7, we can see a properly filtered set of discharges from both campaigns. Upper part represents the NBI energy influence on neutron counts in L-mode discharges. The bottom pictures represents H-mode discharges.
Linear fits are:
L-mode data: $counts = (23,7 \pm 0,7) \cdot E_{NBI}$,
H-mode data: $counts = (29,8 \pm 0,6) \cdot E_{NBI}$.

The result from comparing these curves is, that given the same plasma heating setup (NBI parameters), the achievement of H-mode leads to clearly higher fusion rate. From our curves, it is specifically about 25% higher neutron yield. However, specific numbers need to be taken with great caution just from that point of view, that there are several H-mode types that affect the confinement in a different way. For example, type I ELMy H-mode should lead to higher energy confinement than type III. In the next paragraph, we will demonstrate a "H-mode influence" in more detail.

At the COMPASS tokamak, to identify the "plasma mode" of specific discharge the measurement of H-alpha line intensity evolution is used. For the comparison of H alpha signals, we used data from the campaign "CC18.04 - RMP ELM mitigation". As the name suggests, here the resonant magnetic perturbations were used to mitigate ELMy edge instabilities. In this campaign, in an effort to achieve ELMy H-modes, different types of "plasma confinement modes" from L-mode to ELMy H-modes with the same or very similar other plasma and tokamak conditions was generated. Thus, for the demonstration of plasma mode influence on neutron yield, 3 discharges from this campaign with the same (or almost the same) plasma and tokamak parameters were chosen, specifically these with very different neutron yield. Main parameters of these 3 representative discharges are in the table 3.1.

As we can see from the table, parameters are almost the same including e.g. deuterium gas puff. Just plasma density n_e in the third discharge is about 60% higher, we will come back to density influence very soon. This n_e is the

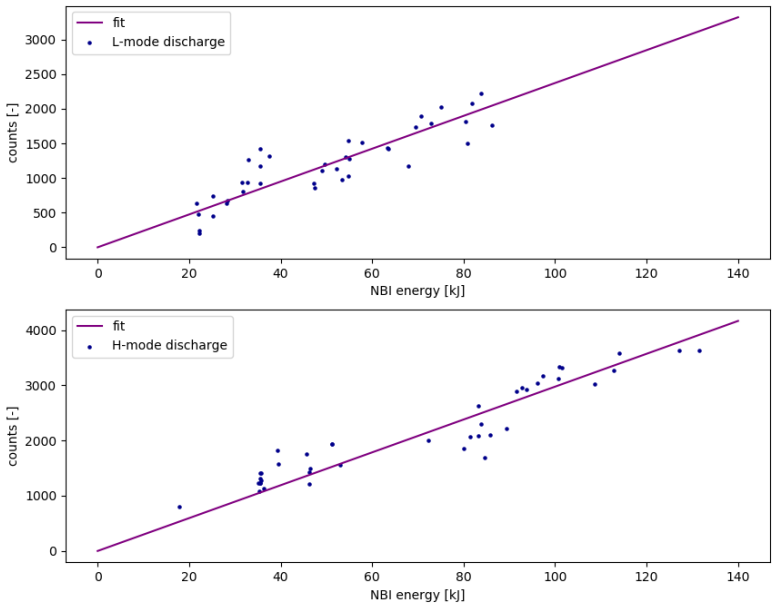

Figure 3.7: Comparison of L-mode and H-mode discharges.

mean electron volume-averaged-density in the time window with NBI on.

The one quite obvious difference is shown by H alpha diagnostics, figure 3.8. The bottom part corresponds to dis. #15510 with neutron $counts = 301$, where it is quite obvious, that plasma in this discharge was in L-mode. The middle part corresponds to dis. #15514 with much more neutron $counts = 1035$. Here the plasma behaves as just before the transition to H-mode. Respectively, it looks like many L-H and H-L transitions occurring rapidly one by one. This happens quite often and it can be theoretically explained as follows: Reaching H-mode means to trigger H-mode threshold heating power, as was discussed in 1.3.1. This should lead to higher plasma density, higher plasma density then leads to higher H-mode threshold and this fact can trigger reverse transition H-L mode. In general it means that the plasma stays somewhere at the boundary of H-mode and L-mode. Unfortunately, the density measurement is not fast enough to follow these changes. Anyway, there is a lot more neutron yield, which could lead us to the idea, that this regime for sure has a better confinement than the L-mode. In fact it could also be it was in the very beginning actually type III ELMy H-mode with very high frequency. From the view of H alpha it can not be said unequivocally, but it could explain the significant rise of neutron yield.

The upper part represents discharge #15524 with the exemplary plasma ELMy H-mode, where the neutron yield is the highest, neutron $counts = 1453$. This ELMy H-mode should be type III, because heating power was almost the same as in discharge #15514, although the ELM frequency looks like more

type I ELMs. Plasma was clearly in the H-mode regime for the whole NBI operational period, this fact could explain additional rise of neutron yield. It is quite complicated to compare just "L-mode" and "H-mode". Namely, for example in the comparison of 2 sets of discharges fitted with linear curves presented above in the text, one set with "H-mode" discharges and second with "L-mode" discharges, discharges #15510 and #15514 would be both categorized in the "L-mode" set (speaking of tag to mark H-mode discharges in COMPASS database), though they seem quite different, as was presented in the previous paragraph.

Together, it is very complicated to draw some specific numbers or results, anyway the visible influence of "plasma confinement mode" on the number of fusion reactions (here presented by measured neutron yields) is registered.

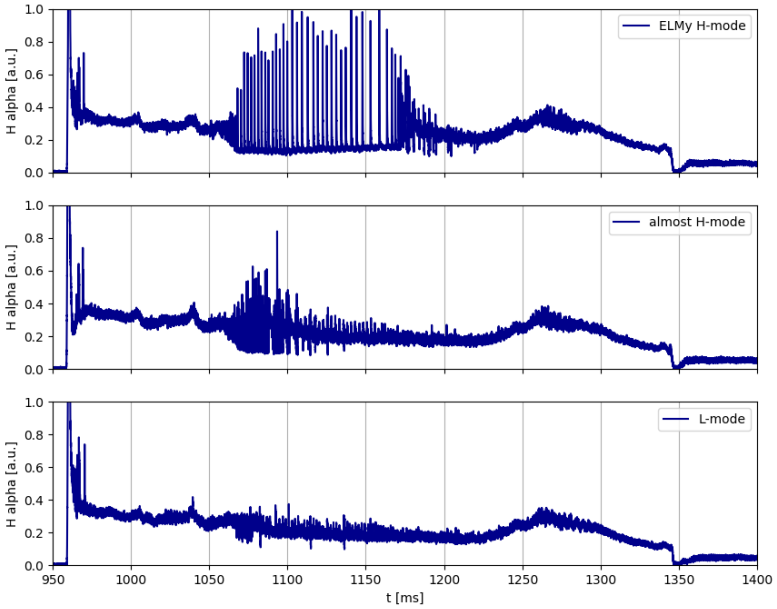

Figure 3.8: Comparison of H alpha lines.

parameter	unit	#15510	#15514	#15524
$counts$	[-]	301	1035	1453
E_{NBI}	[kJ]	37,4	38,6	38,6
I_p	[kA]	230,8	230,6	231,0
n_e	[1e19 m-3]	3,2	3,5	5,7
B_T	[T]	-1,15	-1,15	-1,15
t_{dur}	[ms]	368,8	368,7	368,6
t_{NBI}	[ms]	100,2	100,1	100,2

Table 3.1: Comparison of plasma parameters.

3.6 Influence of plasma density

Back to plasma density, which we skipped a little in the previous section. In three reference discharges described in previous section, we have used volume-averaged electron density (as it is usual in tokamaks for describing plasma density) using thomson scattering diagnostics. For neutron generation, plasma ion density should be analysed instead of electron density. But in plasma, n_i usually follows n_e, so for example higher n_e means basically also higher n_i, because plasma is quasineutral.

The simple theory of the particle collisions (see section 5.1) leads to the result, that higher n_e should clearly lead to higher neutron yield. In the cases of NBI heating plasma in tokamaks, it turns out, that it is more complicated than this simple assertion. Let us get back to previous 3 reference discharges. Here, mean n_e during NBI period was $3,2 \rightarrow 3,5 \rightarrow 5,7$ [1e19 m-3] and its corresponding neutron counts $301 \rightarrow 1035 \rightarrow 1453$, see the table 3.1. Assuming that the values are correct we should see significant density raise between first two discharges according to much higher neutron yield. Another 'strange' behaviour is presented in the figure 3.9 (discharge #15524 - the third column in table 3.1, where we can see density time evolution and corresponding neutron yield time evolution. We can clearly see, that n_e is significantly rising, but neutron yield still decreases over time. In the next rows, we will clarify this behaviour.

In NBI heated tokamaks, there needs to be recognized mainly between "thermal fusion neutrons", which rise from random thermal collisions (this is profitable fusion the triple product is describing) and between beam-target (BT) neutrons, which are produced by direct fusion of fast deuterium ion (ionised deuterium atom from NBI beam, which did not manage to thermalize (energy up to 40 keV)) and with thermal deuterium ion (plasma target - energy of a few hundreds of eV). There is also a possibility of beam-beam fusion neutrons, but their contribution is generally marginal. [19]

These BT neutrons are a significant part of neutron yield, (e.g. JET NBI discharges has a thermal neutrons to BT neutrons ratio very generally speaking about 1:1 [19]). In much smaller tokamak COMPASS, where plasma temperatures are approx ten times lower than in JET, it can be assumed, that BT neutrons form the more significant part than thermal fusion neutrons. The energy of neutral particles produced by NBIs is choosed, so that these particles can penetrate the plasma and be ionised in the plasma core ideally. This depends on plasma size and also on plasma density strongly. It means, that higher n_e decreases the penetration of NBI beam and as it was also discussed in [19], this negative effect overwhelms the higher n_e (which is in itself a positive fact for fusion rate).

In this state, comparing discharges #15514 and #15524 just from the view of density, it should lead to decreasing neutron yield and not the other way around. To clarify this behaviour, we will use the help of other diagnostics in

the next section.

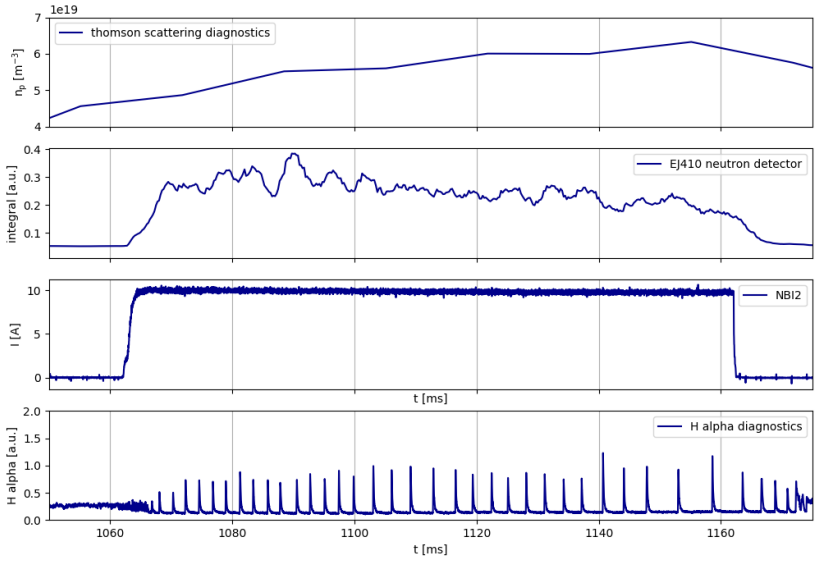

Figure 3.9: Density evolution during ELMy H-mode.

3.7 Influence of plasma temperature, plasma energy and radiation loss

In previous section, we have discussed the influence of very important parameter n_e. But alone it can not clarify the fusion performance behaviour. Here, we will add to our analysis the view of the energy flows in plasma, which seem be very important also.

The table 3.2 represents three another plasma parameters: plasma electron temperature t_e measured by thomson scattering (TS) diagnostics (the same diagnostics measures also n_e), plasma energy W_p measured by diamagetic diagnostics and radiation loss power P_{rad} measured by bolometric diagnostic set. All these three parameters somehow describe energy flows in plasma in time and they affect each other more or less. In the table 3.2, mean values of these parameters during NBI operational period are calculated. All of these parameters are more or less connected to each other, because W_p should be proportional to n_e and t_e, P_{rad} is a partly proportional to a P_{loss} (total energy power loss), which is basically W_p/τ_E etc. In reality, it seems to be much more complicated.

If we could talk about individual influence of each of these parameters on fusion performance, then rising of t_e and W_p should lead to better fusion performance, on the other hand rising of P_{rad} should lead to decrease in the

fusion reaction rate. If we compare these parameters between #15510 and #15514, all of them are improved, so the rising of neutron yield is in place. However, neutron yield increased approx three times, while these parameters did not increase so much in relative values. Anyway, if we compare #15514 and #15524, there is an increase of t_e and significant increase of W_p, which should lead probably to a very significant rise of neutron yield, but this effect is probably reduced by a significant increase of n_e and P_{rad}, thus we only see about 40% increase of neutron yield.

This once again shows that there are many parameters connected and our COMPASS neutron database is too much diverse to try to make some specific mathematical prediction based on fitting our neutron data. Anyway, we can quite apparently confirm based on our data, that H-mode generally leads to a rise of confinement time of NBI fast ions and to a better fusion performance.

parameter	unit	#15510	#15514	#15524
counts	[-]	301	1035	1453
n_e	[1e19 m-3]	3,2	3,5	5,7
t_e	[eV]	726	757	793
W_p	[kJ]	5,6	6,1	8,5
P_{rad}	[kW]	36,3	30,4	58,8

Table 3.2: Comparison of plasma parameters, stage 2.

Speaking of time evolution, the situation also looks complicated and unclear, see the figure 3.10. L-mode discharge #15510 has during the whole NBI operational period approx. constant neutron yield, see the last row in the figure 3.10. On the other hand, discharges #15514 and #15524 have a declining trend in neutron yield over the NBI operational period. Comparing #15510 and #15514 time evolution, the gradient of W_p is a little bit higher in #15514 than #15510 and also P_{rad} decreases a little bit slower in #15514. It could theoretically support the decreasing trend of neutron yield in #15514. On the other hand, #15524 has intensive rising of W_p, it should theoretically lead to increase of neutron yield, but simultaneously the P_{rad} intensively rises as well.

It means that apparently H-mode is beneficial for increased confinement time of NBI fast ions and increasing the temperature, however, the increase in the density and perhaps increased accumulation of impurities and other effect eventually lead to gradual decay of the neutron yield.

3.8 Summary of dependencies

As was presented in the previous sections, it is very complicated to tell exactly, what is the reason of the large scatter in neutron yields in discharges

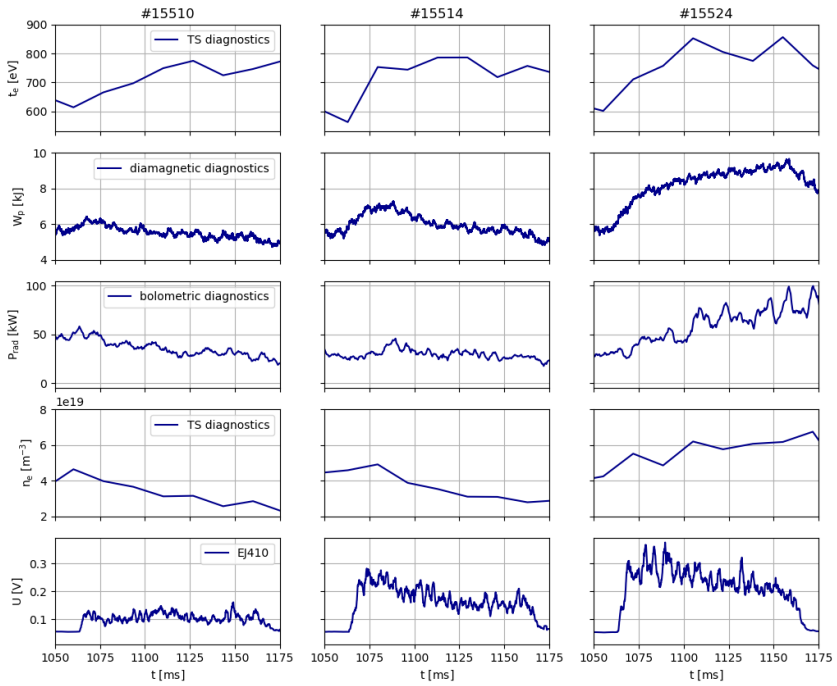

Figure 3.10: Comparison of plasma parameters between discharges #15510, #15514 and #15524.

with very similar parameters. It seems, that small changes can lead to a big change of fusion performance.

Thus, we should compare just the discharges with the absolutely same NBI parameters like #15514 and #15524. Here, we have measured about 40% larger neutron gain. It could correspond to the achieved ELMy H-mode in #15524. This 40% neutron growth is consistent with the result of comparing curves of L-modes vs H-modes discharges in figure 3.7, back in section 3.5, where we have assumed about 25% more neutron gain. If we consider high variability of discharges, these two results are close enough.

A significant rise of W_p in #15524 also nicely corresponds to H-mode theory. In the latest results from JET ([19]), they have measured a significant gain of BT neutrons despite of the rise of n_e, because the rise of t_e and W_p overcame worse NBI beam penetration to plasma. The same result can be interpreted in our situation very nicely as well.

Summarizing this, the far most important parameter to have an effect on fusion performance here at COMPASS tokamak is the NBI heating power. In the second place, the neutron gain can be enhanced by achieving a H-mode plasma confinement regime. The influence of other parameters are either marginal or are very complicated to measure.

Chapter 4

Estimation of wall shielding efficiency in COMPASS and COMPASS-U tokamak

In the near future, the Institute of Plasma Physics will start to build a new tokamak COMPASS Upgrade. This tokamak will be built in the same place instead of the COMPASS tokamak. It is expected, that COMPASS-U will have up to factor of $\sim 10^4$ higher neutron fluxes than COMPASS. It can thus be assumed, that existing wall shielding would not be sufficient. In this chapter the measurement of neutron fluxes behind the main shielding wall of the COMPASS experimental hall is presented. The results lead to determination of the neutron attenuation coefficient of the COMPASS shielding wall. Then the equivalent dose of neutron radiation in the neighbourhood of the COMPASS and COMPASS-U tokamak experimental hall is estimated.

4.1 Experimental setup

The measurement was performed in December 2019 during campaign CC21.06 between discharges #19850 - #19917. We have used the neutron scintillation detector NuDET placed behind the main wall around the tokamak COMPASS. For data collection we have used OWON oscilloscope XDS3202A.

To estimate neutron wall attenuation coefficient, data measured by the same detector NuDET connected to the different setup (oscilloscope NI PXI 5114) was also processed. The detector in this case was measuring neutron fluxes in May 2018 during campaign CC19.05 in the range of discharges

#16893 - #17099 inside the experimental hall of the COMPASS tokamak.

4.2 Estimation of neutron wall attenuation coefficient

The main shielding wall around the COMPASS tokamak is made from concrete of a special type with a thickness of 60 cm.

4.2.1 Measurement technique

It would be relatively easy to gain neutron wall attenuation coefficient, if we would have measured neutron counts inside and outside of the wall at the same time (in the same discharges). But due to technical issues this „double measurement“ was not realised. However, it appeared, that there is another way, how to work around this problem and use neutron counts inside and outside the hall from different discharges.

Besides NuDET detector, which is often used for special measurements like this, neutron diagnostic on COMPASS uses another scintillation detector EJ-410 from the Eljen Technology company. This detector does not measure individual neutron counts (due to parameters of the data acquisition system ATCA 2). The signal consists of pile-uping of many individual neutron peaks, as we can see in the figure 4.1. But it's quite obvious, that the integral of the signal is proportional to the number of neutron counts. Another important fact is, that the detector EJ-410 operated with the same setup (always in the same position around tokamak, with the same lead shielding, data acquisition system, with fixed voltage on PMT, ...). Due to these two facts (signal proportional to number of counts, stable setup) it was clearly shown, [20], that we can use integral of the EJ-410 signal as a figure of merit. Thus we can compare neutron counts from different discharges.

The principle is schematically shown in the figure 4.2. All we need is to determine (purple) linear curves of dependency of neutron counts on the integral of EJ-410 in the case of a detector inside the hall with tokamak and in the case when detector was operated outside, too. These linear curves

$$c_i = k_1 \cdot I, \tag{4.1}$$

$$c_o = k_2 \cdot I, \tag{4.2}$$

where c_i, c_o are number of neutron counts inside (outside) the hall, I is the integral of EJ-410 signal, determine parameters k_1, k_2. Their ratio equals to

neutron wall attenuation coefficient K_n

$$\frac{k_1}{k_2} = \frac{c_i}{c_o} \equiv K_n. \tag{4.3}$$

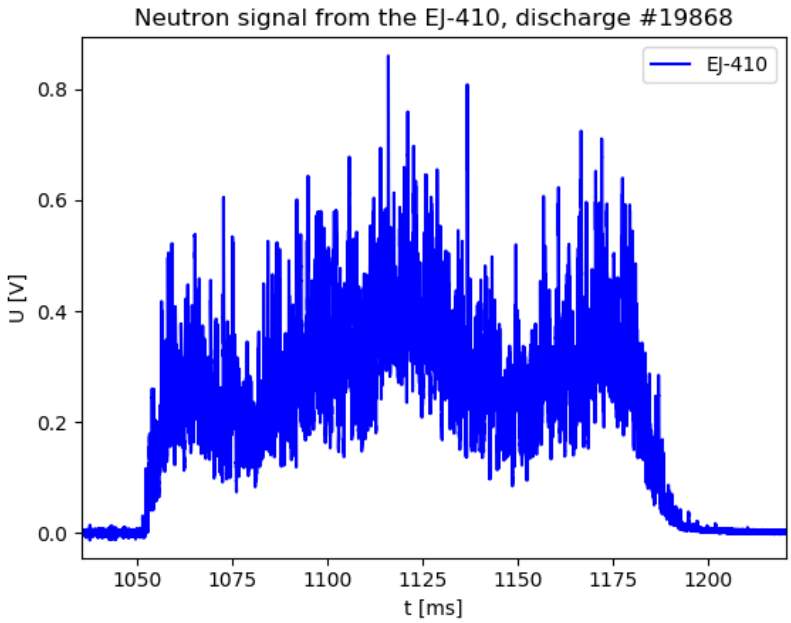

Figure 4.1: Example of the piled-up neutron signal from the EJ-410, discharge #19868.

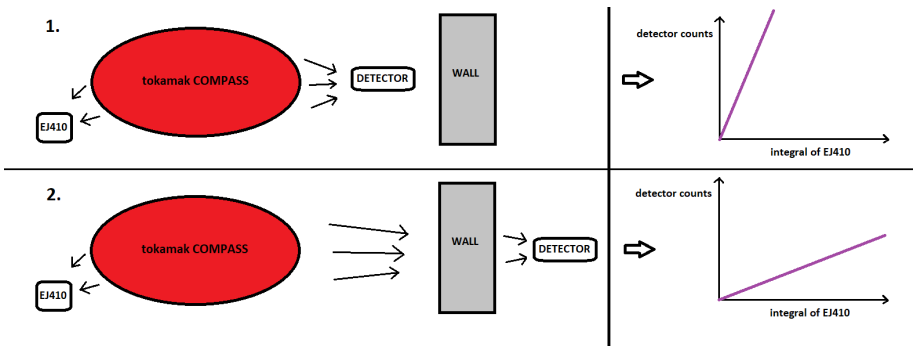

Figure 4.2: Schematic picture illustrates two different situations - inside/outside measurement.

4.2.2 Results

Figure 4.3 shows individual discharges from the campaign CC19.05 conducted in May 2018, when NuDET detector was placed inside the hall with the COMPASS tokamak. We can see quite obvious linear dependence. Final linear fit (purple) was calculated as

$$c_i = (334.22 \pm 7.37) \cdot I. \tag{4.4}$$

Figure 4.4 shows individual discharges from campaign CC21.06 conducted in December 2019, when NuDET detector was placed outside the hall with COMPASS tokamak. There was a smaller number of usable discharges for our purpose, but linear dependence is still visible. Final linear fit (purple) was calculated as

$$c_o = (4.00 \pm 0.13) \cdot I. \tag{4.5}$$

Finally neutron wall attenuation coefficient K_n defined in eq. 4.3 was calculated as

$$K_n = 83.56 \pm 3.28 \simeq 84. \tag{4.6}$$

This number means, that for every neutron, which passed through the wall, there were 84 neutrons absorbed in the shielding wall or reflected back to the interior of the experimental hall. The bigger the K_n is, the better the wall shields surrounding systems and workers. The main factor, which was not taken into account, is probably the influence of the wall on neutron energy spectra. The concrete shielding wall naturally moderates neutrons and thus neutron capture rate by lithium in NuDET detector can dramatically increase, as we can see in the figure 2.1. So this result should be better understood as the bottom estimation of neutron wall attenuation ability (in the meaning of minimal wall shielding ability).

These results were also confirmed later in 2021 in summer school, where simultaneous measurement with one NuDET inside and the second one outside the main shielding wall around the COMPASS tokamak was released. The results were very similar.

4.3 Equivalent dose of neutron radiation

Knowledge of the neutron energy spectra, to which the detector is exposed, is the key information for correct determination of neutron fluxes and thus for calculating equivalent dose. It is due to a wide range of the value of the cross section for the reaction of neutron with lithium. But we can calculate very strong upper estimate of the equivalent dose, which worker will be exposed to behind the wall of the tokamak.

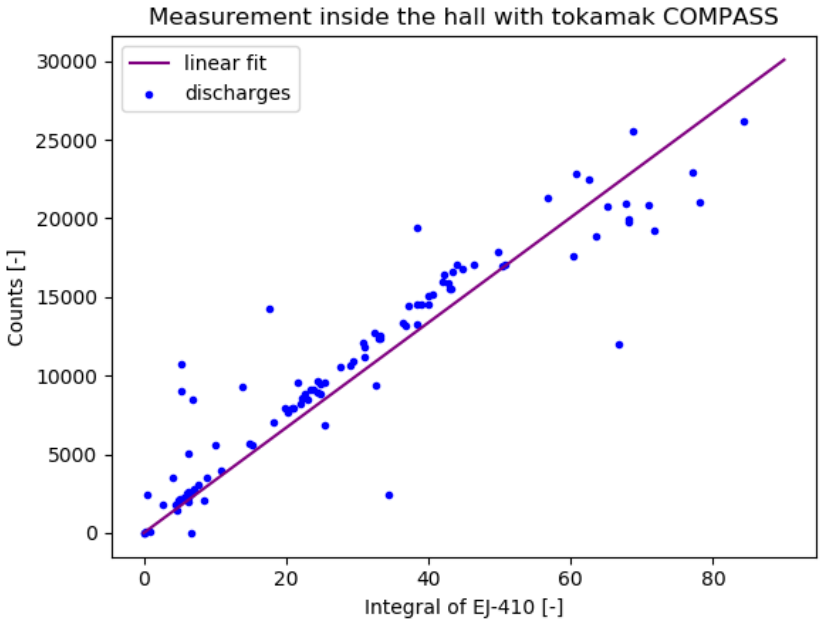

Figure 4.3: Linear fit for inside measurement.

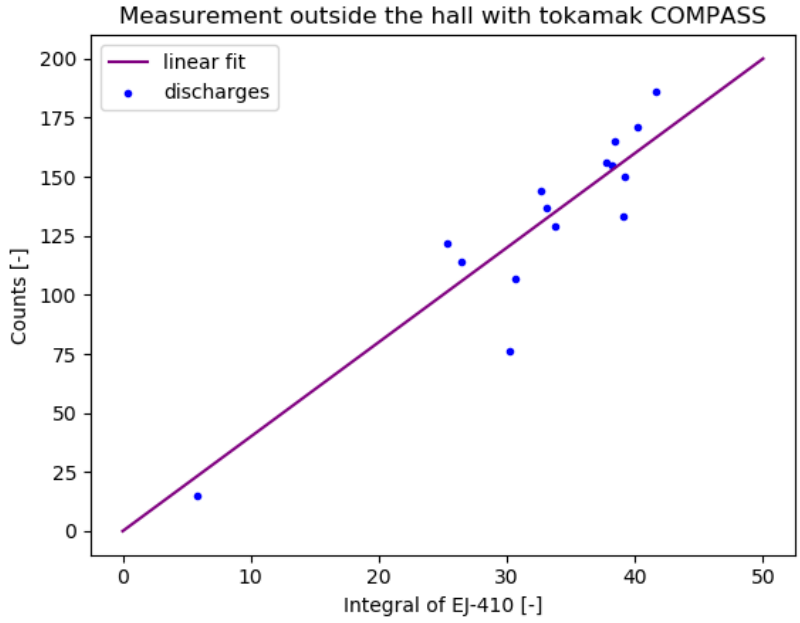

Figure 4.4: Linear fit for outside measurement.

The assumptions are as follows:
1. 1500 discharges during a year, all with 30000 neutron counts on NuDET inside. This is a bit higher than maximum measured neutron flux in May 2018 (maximum was cca 27 000 neutron counts).

2. Neutron wall attenuation coefficient $K_n = 84$. As stated above, the true K_n should be probably higher due to moderating neutrons by wall.
3. The cross section of the human body (worker) is about 1 m^2 and the weight is about 80 kg.
4. All passed neutrons through the shielding wall have energy 25 keV. The reason is as follows. Attenuation coefficient K_n says to us, that only one neutron passed through the wall on each 84 neutrons, which are absorbed (or reflected back). The neutron absorption in the wall in particular takes place in such a way, that fast neutrons are slowly moderated during elastic collisions with material nuclei. After slowing down on ideally thermal energies, neutrons are absorbed in the material (because of high cross section of absorption for slow/thermal neutrons). It can be thus assumed, that the one neutron passed through the wall will be strongly moderated too in each case. For strong upper estimate let's say the passed neutrons are minimally 100 times slowed, this is energy of 25 keV. The smaller the energy will be, the smaller will be the absorbed dose. So this is ideal for strong upper estimate of the absorbed dose. The cross section for nuclear reaction of neutron with 25 keV with ^{6}Li is about 1 barn, based on figure 2.1.
5. Radiation weighting factor $W_R = 10$. It corresponds approximately to neutron with energy 25 keV, [17].
6. All neutron radiation, which entered into the human body, is completely absorbed, none goes through.

4.3.1 Equivalent dose behind the wall of the COMPASS tokamak

For the estimation of equivalent dose, the efficiency of detection of 25 keV neutron by NuDET detector was first calculated. It is basically 1000 times lower than for thermal neutrons, because the cross-section is approx. 1000 times lower, if we consider NuDET detector as thin target approximation. Thick target approximation should lead to a bit higher detection efficiency, so the final equivalent dose would be a bit lower, see theory in section 5.1. After this it is simple to calculate number of neutron counts for the whole year. Finally equivalent dose for tokamak COMPASS H_C, eq. 1.3, was determined as

$$H_C = 596.25 \quad \mu\text{Sv/year}. \tag{4.7}$$

Allowed equivalent dose for worker with ionizing radiation is 50 mSv/year (for general public 2 mSv/year). H_C **is than 84x lower than set limit.** Let's take note, that it is strong upper estimate. The true equivalent dose should be much lower. **If we consider thermal neutrons (0.025 eV) behind the wall instead of neutron energy of 25 keV, it should lead to decrease of equivalent dose by many orders of magnitude**.

4.3.2 Equivalent dose behind the wall of the COMPASS-U tokamak

For the estimation of equivalent dose for COMPASS-U the same assumptions like for COMPASS were used, but with two changes. Every discharge will cause $\sim 3 \cdot 10^9$ neutrons registered in NuDET detector inside (which is actually to much for NuDET to handle). It means up to 10^5 higher amount of neutrons from COMPASS-U than from COMPASS (by 10^4 higher neutron fluxes and the duration of NBI heating phase will be 10x longer).

The second change is in the neutron attenuation coefficient. The shielding wall of COMPASS-U will be composed of old 60 cm thick concrete wall from COMPASS and from additional 90 cm thick layer of new concrete with boron. So the COMPASS-U will be shielded by 150 cm thick concrete wall. This wall should reduce neutron fluxes by around six orders of magnitude ($K_n = 10^6$), see the figure 4.5. Note, that the reduction of absorbed dose by 60 cm thick concrete is about 2 orders of magnitude in this figure, which well corresponds with our measurement of neutron attenuation coefficient, so the use of the results from this figure from [4] is reasonable.

The equivalent dose for COMPASS-U is then

$$H_{C-U} = 5.01 \quad \text{mSv/year}. \tag{4.8}$$

This equivalent dose is 10x lower than the set limit. Again, it is very strong upper estimate. The true equivalent dose should be much lower. Moreover, the structures of the COMPASS-U will have radically higher radiation shielding ability by itself than structures of COMPASS and the additional boron concrete will probably have better shielding properties than ordinary concrete. These facts are not taken into account in this calculation and thus should rapidly decrease the true equivalent dose, too. **If we consider thermal neutrons (0.025 eV) behind the wall instead of neutron energy of 25 keV, it should lead to decrease of equivalent dose by many orders of magnitude**. Also, the COMPASS-U tokamak will not operate at full parameters in many campaigns at all, so the real equivalent dose should be similar as at the COMPASS tokamak.

It is worth mentioning, that these estimations do not take into account different equivalent doses from RE campaigns, where strong neutron yields and also HXR yields are presented as well.

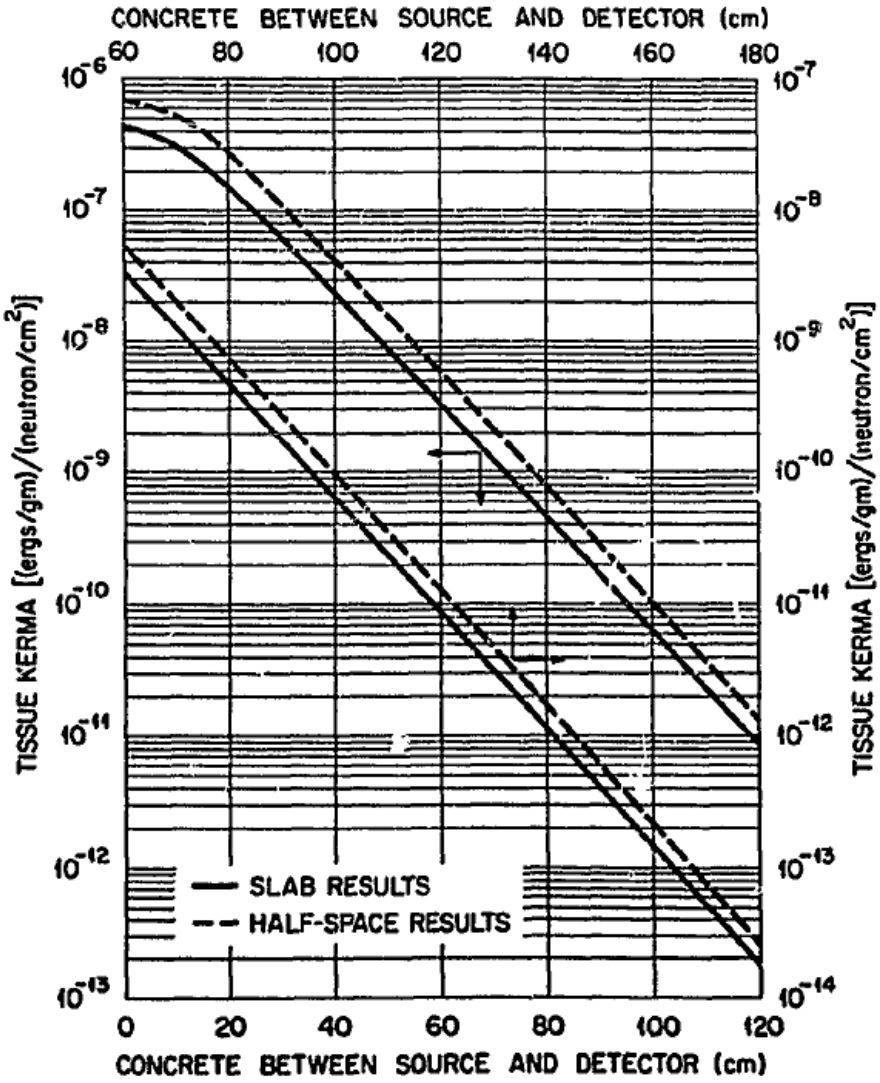

Figure 4.5: Reduction of absorbed dose by ordinary concrete shielding from 3 MeV incident neutrons, [4].

Part II

Measurement of photoneutrons at the COMPASS tokamak

Chapter 5

Brief theoretical background

This chapter contains basic informations about the mathematical concepts and physical phenomena used in the next chapters and thus can help the reader in understanding the text.

5.1 Cross section of the nuclear reaction

The knowledge of nuclear reactions respectively the conditions, under which nuclear reactions occur or occur often enough, is the key information. For example, the thermonuclear fusion research is trying to reach these optimal conditions of especially D-D and D-T nuclear reactions. The main parameter, which describes these conditions, is the cross section σ of nuclear reaction defined

$$\sigma = \frac{R}{N\Gamma}, \tag{5.1}$$

where R [s^{-1}] is a frequency of nuclear reaction, N [$-$] is the number of the atomic nuclei of the motionless target and Γ [$m^{-2}s^{-1}$] is the flux of shelling particles hitting the target. The unit of σ is m^2, it is imaginable approximately like the effective area, which the particle must strike in order the nuclear reaction to occur. Because of very small values the usually used unit is barn (1 barn $= 1 \cdot 10^{-28}$ m^2), see e.g. [21].

The above presented definition is actually based on "thin target" approximation. It represents the situation, where the shelling beam is almost unchanged after the interaction with the target. It means minimal interactions of shelling

particles with the target, where the reasons may be different (low cross-section, low thickness of the target, etc.). On the other hand, the equation representing "thick target", which visibly affects shelling beam, is

$$N_0 = \frac{\Delta N}{1 - e^{-n\sigma d}}, \tag{5.2}$$

where ΔN is the number of reactions in a thick target of the density n and the thickness of d caused by the number of shelling particles N_0, where σ is the cross-section of a specific reaction.

If $n\sigma d << 1$, we can approximate $e^{-n\sigma d}$ by $1 - n\sigma d$ (Taylor series) and the thick target definition transforms into the thin target approximation, whose version is the equation 5.1. [22]

5.2 Fourier transform

Generally we can imagine some function $z(t)$ like continuous superposition of the functions sine and cosine with different frequencies f:

$$z(t) = \frac{1}{2\pi} \int_{-\infty}^{+\infty} Z(\omega) \mathrm{e}^{i\omega t} d\omega, \tag{5.3}$$

where $\omega = 2\pi f$. This is called the inverse Fourier transform. Usually we are interested, which frequencies are dominant for the given function $z(t)$. For this purpose, the function $Z(\omega)$ called Fourier transform needs to be calculated. Fourier transform can be expressed like

$$Z(\omega) = \int_{-\infty}^{+\infty} z(t) \mathrm{e}^{-i\omega t} dt. \tag{5.4}$$

In other words, Fourier transform converts the function $z(t)$ from the time domain to the frequency domain (frequency spectrum).

In the next chapter, we will use the theory of Fourier transform in order to create a frequency filter for neutron/γ signal discrimination. Our function of interest is the exponential function $z(t) = A \cdot \mathrm{e}^{-\frac{t}{\tau}}$. By using eq. 5.4 we can simply gain

$$Z(\omega) = \frac{A}{\frac{1}{\tau} + i\omega} = \frac{A(\frac{1}{\tau} - i\omega)}{\frac{1}{\tau^2} + \omega^2}. \tag{5.5}$$

The absolute value gives us the frequency spectrum of the exponential function $z(t)$

$$\mid Z(\omega) \mid = \frac{A}{\sqrt{\frac{1}{\tau^2} + (2\pi f)^2}}. \tag{5.6}$$

For more details about Fourier transform see [23].

5.3 Runaway electrons

One of the up to date hot topics in the fusion tokamak research are runaway electrons. Runaway electrons are electrons, which are accelerated to the relativistic velocities. REs usually appear during disruptions in the tokamaks, when strong electric field is suddenly induced. Basically electrons are more accelerated than braked by thermal collisions and so runaway electrons arise. Beam of the REs can damage plasma facing components. In chapter 6, we are focusing on the measurement of HXR radiation and photo-neutron radiation caused by the collisions of REs with plasma facing components.

5.3.1 RE generation mechanisms

To mitigate runaway electrons in the tokamak plasma, the key information is to know, how REs were created. Unfortunately, today is well known more than a one way, how REs could be generated. The general theory of RE generation describes three main mechanisms - Dreicer mechanism, hot-tail mechanism and avalanche mechanism. In the next lines, a very brief description of each of these mechanisms is presented.

Dreicer mechanism

Dreicer mechanism (or primary generation) stands on the comparison of the accelerating electric field E and the collisional friction (drag) force. Probably the clearest version of equation of motion is the one with defined Dreicer field E_D and Chandrasekhar function ψ

$$\frac{\partial v}{\partial t} = \frac{eE}{m_e} - \frac{2e}{m_e} E_D \psi(v/v_T), \tag{5.7}$$

where v, v_T and m_e are velocity, thermal velocity and electron mass. Chandrasekhar function is a very special integral function with the maximum for $v = v_T$. It means, that the friction is the most intense, when electron has plasma thermal velocity. Rising velocity thus leads to friction decrease, which can lead to a generation of the runaway electrons.

Plasma parameter E_D is defined

$$E_D = \frac{n_e e^3}{4\pi\epsilon_0^2 k T_e} ln\Lambda, \tag{5.8}$$

where n_e is electron density, e elementary charge, ϵ_0 vacuum permittivity, k Boltzmann constant, T_e electron temperature and $ln\Lambda$ is Coulomb logarithm. The lower E_D is, the lower is also a friction force. In the figure 5.1, the illustration of the Dreicer mechanism along with other two RE generation mechanisms is presented. Simply said, a group of electrons with high enough velocities, especially in the plasma conditions with low n_e and high T_e along with high accelerating electric field can become a group of REs. [5]

Hot-tail mechanism

Hot-tail mechanism has the same basics as Dricer mechanism, but especially it describes behaviour of REs in the more specific situations. A typical situation is, when the plasma is rapidly cooling. It can be caused for example by High-Z gas puff into the plasma, see the next section. This situation is nicely illustrated in the figure 5.1. Rapid plasma cooling leads to decreasing of temperature mainly of bulk plasma around thermal velocities, but the always presenting hot (high velocities) tail in Maxwellian electron distribution is almost untouched, because collisional drag force almost does not work for these electrons (low value of Chandrasekhar function). This will outweigh the impact of naturally rising value of E_D (lower T_e), simply said. [5]

Avalanche mechanism

Avalanche RE generation mechanism is also well illustrated in the figure 5.1. The principle is simple. Electrons with very high energy (REs) can transform by Coulomb collision with thermal electrons a significant part of their energy and thus to make a new RE electrons and still stay in RE regime. This process can lead to an intensive increase of number of REs, but also to a decrease of energy spectra of these REs. Good conditions are naturally a more focused, concentrated plasma (high gradient of n_e radial profile) and also a time is required (long discharges). Thus this process is supposed to be dominant at big tokamaks like ITER. For more detailed information about physics of runaway electrons in tokamaks, see e.g. [5, 24].

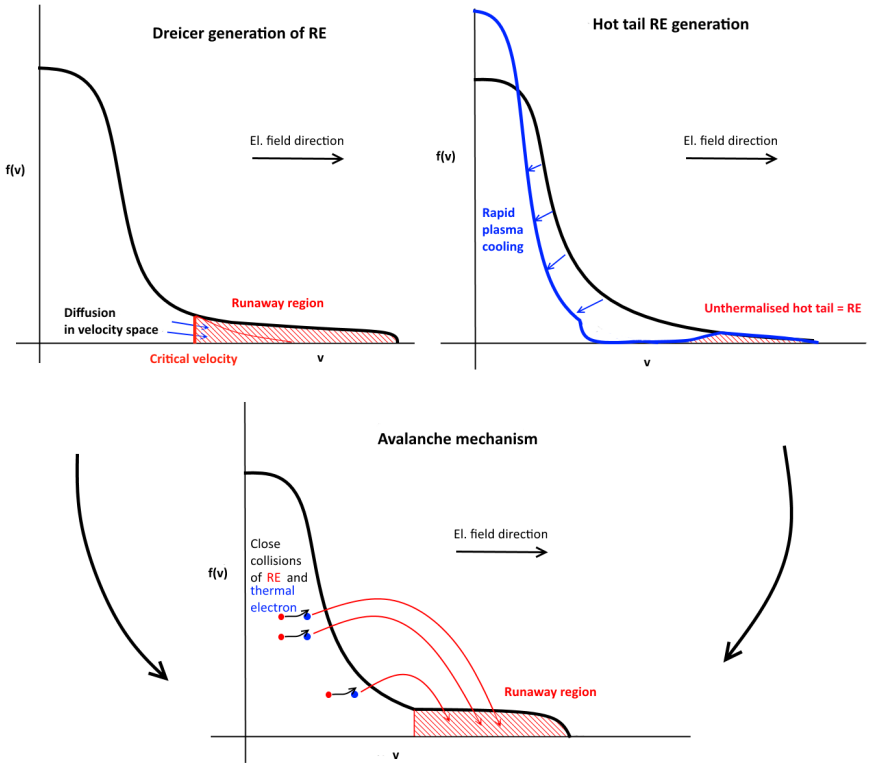

Figure 5.1: Illustration of all three RE mechanisms. [5]

5.4 High-Z element gas puff

It is clearly known, that the injection of gas of high Z like noble gases Ar or Kr has a significant impact on the RE behaviour. One of the usual situation of use is to inject a big amount of high-Z gas during ramp-up phase to boost a hot-tail RE generation mechanism by rapid plasma cooling, because just a little amount of high-Z atoms in the plasma can cause a radiation plasma collapse (disruption). Thus we can study such RE beam and test techniques to its mitigation. [25]

In some situations, a reasonable amount of high-Z gas puff can be theoretically used to "isolate" already presented hot-tail in Maxwellian electron energy distribution and thus to a prevent that other electrons are moved to RE regime and to carry a higher current, which could cause potentially a more damage to the surrounding structures.

In each case, the RE behaviour depends strongly on the **amount** of high-Z gas puff, becasue it significantly affects, whether it triggers a disruption or not. A right amount and a combination of high-Z gas puff with deuterium puff can also lead to a sudden disruption without REs, see [26].

In the following analysis, at COMPASS tokamak, a "non-disruption amount" of Ar or Ne injection followed by a secondary deuterium gas injection has

been recently tested. One of the reasons was to study a better positional stability of RE beam and perhaps also smaller acceleration of RE due to smaller current decay rate. For detailed information about noble gas puff at the COMPASS tokamak, see the paper [27].

5.5 Photo-neutrons

In the next chapters, our interest will be focused on the photo-disintegration nuclear reactions, which produce neutron radiation. This kind of a nuclear reaction can be simply wrote as

$$\mathrm{A}(\gamma, \mathrm{n})\mathrm{B}, \tag{5.9}$$

where γ or HXR photon interacts with a target nucleus A. As a result, a neutron and a different nucleus B is released. This is a typical situation, but in some photo-disintegration reactions more than one neutron can be released or accompanied by proton or alpha particle. [6]

The common attribute for these reactions is, that they are endothermic. The threshold energy of γ photon to induce the reaction varies typically from a few MeV (2.2 MeV with deuterium ([28]) or 1.6 MeV with beryllium ([29])) to a low tens of MeV like with nickel, chrome, iron etc., as we can see in the figure 8.1. Product nucleus is typically a radioactive isotope with its specific γ line.

In a conjunction with the tokamaks, the photo-neutrons are a product of interaction of HXR radiation with the tokamak structures. HXR radiation is generated mainly by a beam of runaway electrons, which collides with tokamak structures, see e.g. [6].

Chapter 6

Measurement of neutrons on the HXR background

Measurement of neutron fluxes on the tokamaks (and other fusion devices) is a very useful tool and especially with growing size and fusion power of the newly built tokamaks, the neutron diagnostics is becoming more and more important. Many of neutron detectors used for measurement of high neutron fluxes like scintillators are also sensitive to HXR/γ radiation. It can be a big disadvantage, but not in the case, that we are able to separate the photons from neutrons (neutron/HXR discrimination).

6.1 Experimental setup

To explore neutron/HXR discrimination capabilities of NuDET scintillator detector we have realised measurement during runaway electron campaign CC22.01 in January/February 2020. Runaway electrons are the strong source of HXR radiation. It was our goal to measure individual HXR peaks and to characterize them. NuDET detector was thus placed behind the main shielding wall around the COMPASS tokamak. Without shielding wall NuDET would not be able to measure individual HXR photons due to too large HXR flux (piled-up signal). NuDET was connected to the OWON oscilloscope XDS3202A with necessary low impedance ($Z = 50$ Ohm) and fast sampling rate from 50 to 250 MHz.

6.2 Measurement of HXR radiation

We have measured with a lot of different oscilloscope input parameters for better understanding of the measured signal and to find optimal oscilloscope setup for these types of measurements. So the data are not self-consistent for some detailed statistical analysis, but we still have obtained important informations about the time dimension and the shape of HXR peaks (see below) at different oscilloscope parameters like vertical resolution, sampling rate and bandwidth.

The shielding wall really shielded HXRs to such an extent, that we could recognise individual HXR peaks, figures 6.1 and 6.2. Numbers of counts vary in a quite wide range from a few thousands up to more than 1 million HXR counts registered in NuDET detector per discharge. The list of the most interesting discharges is presented in the table 6.2. Calculating the estimate of absolute numbers of HXRs generated by the tokamak during discharge is impossible now, because there is still a lot of unknown quantities like HXR wall absorption, HXR spectrum. Unfortunately, neither NuDET sensitivity to HXR is known, respectively it is „low“. It is quite obvious, because NuDET scintillation crystal has a very small volume (40 mm diameter, 4 mm thickness). Typical scintillation crystals for measuring HXRs/γ like NaI(Tl) are manufactured in larger volumes.

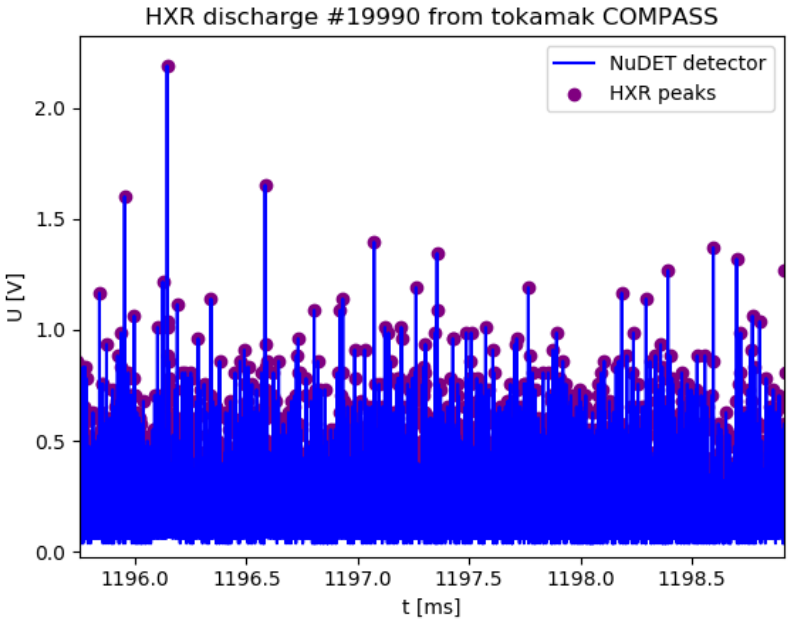

Figure 6.1: Example of the cluster of HXR peaks.

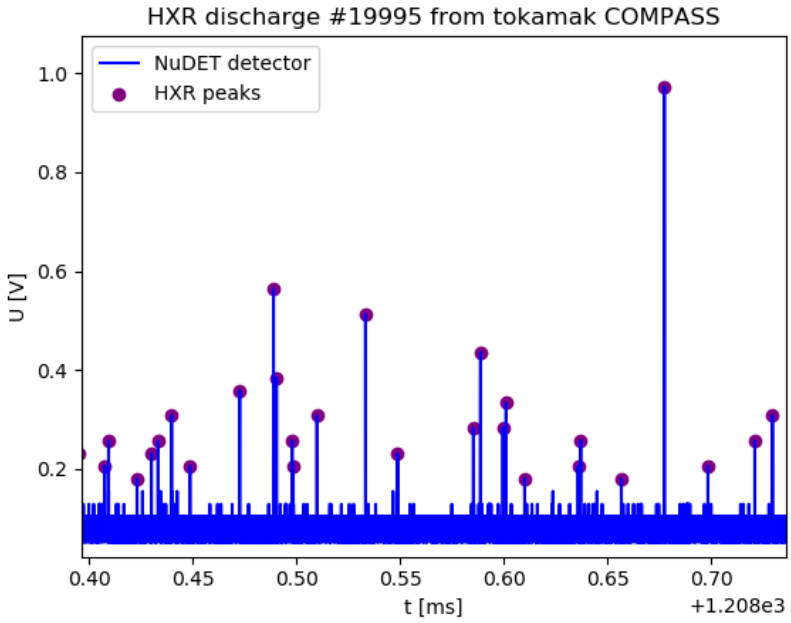

Figure 6.2: Example of HXR peaks (enlarged area).

6.3 Neutrons discovery in the signal

During a detailed study of the HXR signal from NuDET detector we have noticed a few very different peaks. Detailed view on the figures 6.3 and 6.4 shows a substantial difference between representatives of both groups. Notice, that time axis has different units (ns vs μs). Many HXR peaks appear here as a quite big noise of this signal and thus can be interpreted as some random pile-up effect. Due to this fact the analysis of this signal was done.

Representative peaks of both groups were fitted, as we can see on the figures 6.3 and 6.4. Results of fits were compared with the article [30], where author used a similar type of scintillation detector (ZnS(Ag) + LiF). HXR peak was fitted with 1 exponential function (fast component only). Unknown peak was fitted with the sum of 3 exponential functions (fast, slow, ultraslow component). Decay times of individual components are shown in the table 6.1. Ratios of individual decay times are almost the same, ultraslow component is a bit slower, it's probably due to a lot of HXRs in the tail of the neutron peak. Absolute differences are due to different electronics used (PMT, oscilloscope). In conclusion it can be said, that these different peaks are certainly the neutrons and not some piled-up signal.

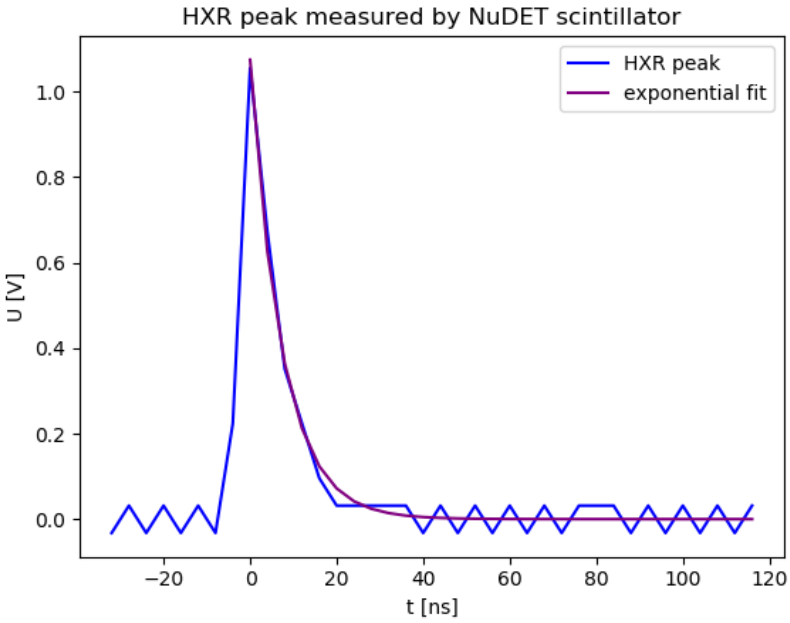

Figure 6.3: Example of the HXR peak.

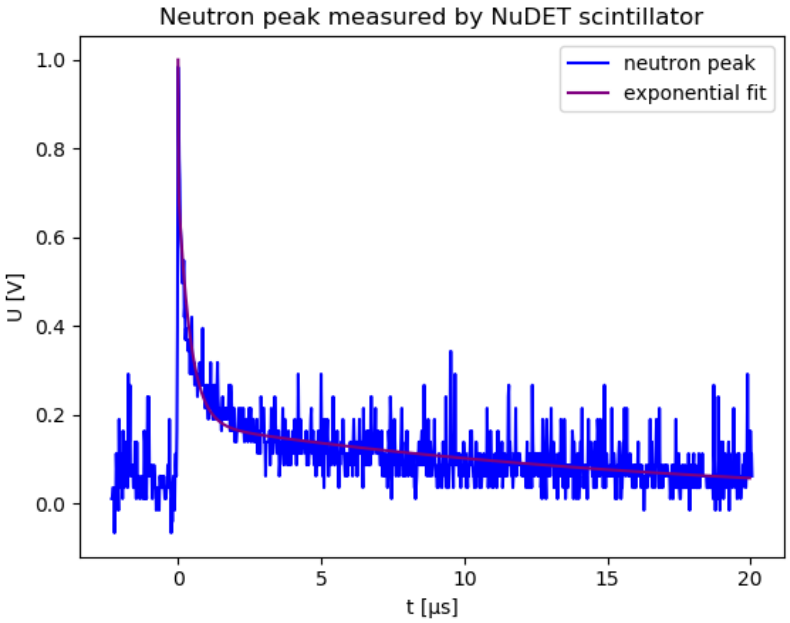

Figure 6.4: Example of the neutron peak.

	OUR FIT [μs]	ARTICLE FIT [μs]
HXR τ_1(fast)	0,008	0,003
neutron τ_1(fast)	0,008	0,003
neutron τ_2(slow)	0,424	0,160
neutron τ_3(ultraslow)	17,367	4,100

Table 6.1: Time decays of HXR and neutron peak.

6.4 Source of neutrons

6.4.1 Neutron/HXR discrimination

For the determination of the neutron source, it was necessary to separate neutron peaks from HXRs. By using Fourier transform of the exponential function (eq. 5.5 and 5.6) the spectral decompositions of neutron/HXR peaks were calculated, figures 6.5 a 6.6. Due to very different decay times their FWHM are greatly different. This fact allowed us to discriminate neutrons from HXR peaks by using 100 kHz lowpass bandwidth filter. As we can see in the figures 6.7 and 6.8, HXR peak is completely filtered out and only ultraslow component of the neutron peak has passed the filter.

This discrimination method is a simple to use and thus it's a good choice in the situations like this with very different decay times of neutron/HXR peaks. In other types of scintillation detectors, e.g. plastic, neutron and HXR peaks can be much more similar, there it would be necessary to use some sofisticated discrimination techniques like Pulse Gradient Anaylsis (PGA), Charge Comaprison Method (CCM), see e.g. [18].

6.4.2 Neutron counts

In the table 6.2, there is a short list with discharges, where we have measured high photo-neutron counts outside the tokamak hall with NuDET detector. Notice, that these amounts of neutrons are in quite similar range compared to D-D fusion neutron counts measured with the same detector in the same setup (behind the COMPASS shielding wall) in the NBI campaign CC21.06, see chapter 4. But in this situation, it is clearly known, that these neutrons do not come from D-D fusion reactions because of the absence of NBI heating power, which is absolutely crucial, as was presented in part I of this thesis.

The presence of neutrons in RE campaigns without NBI power leads nat-

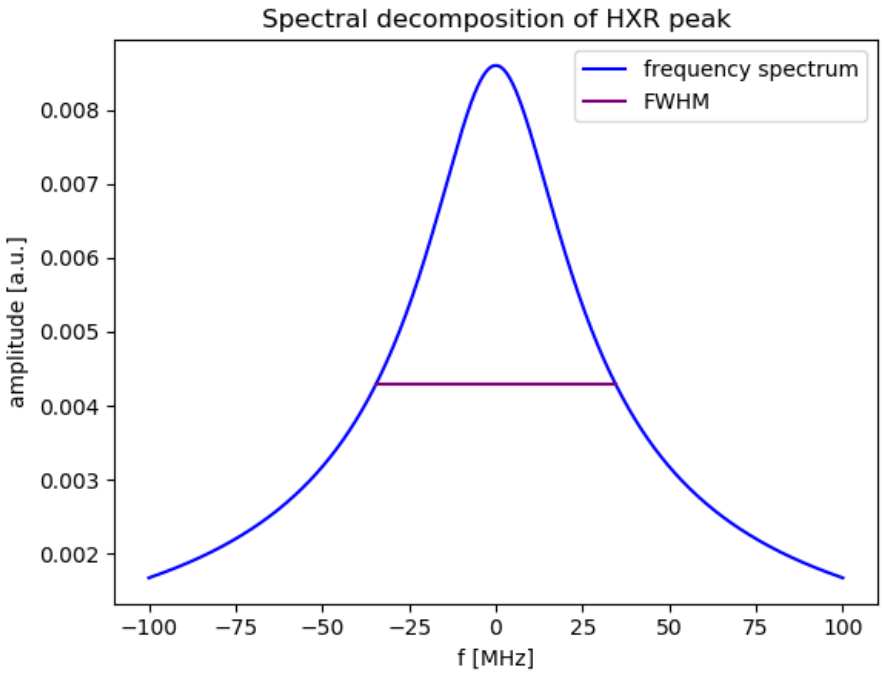

Figure 6.5: Spectral decomposition of HXR peak.

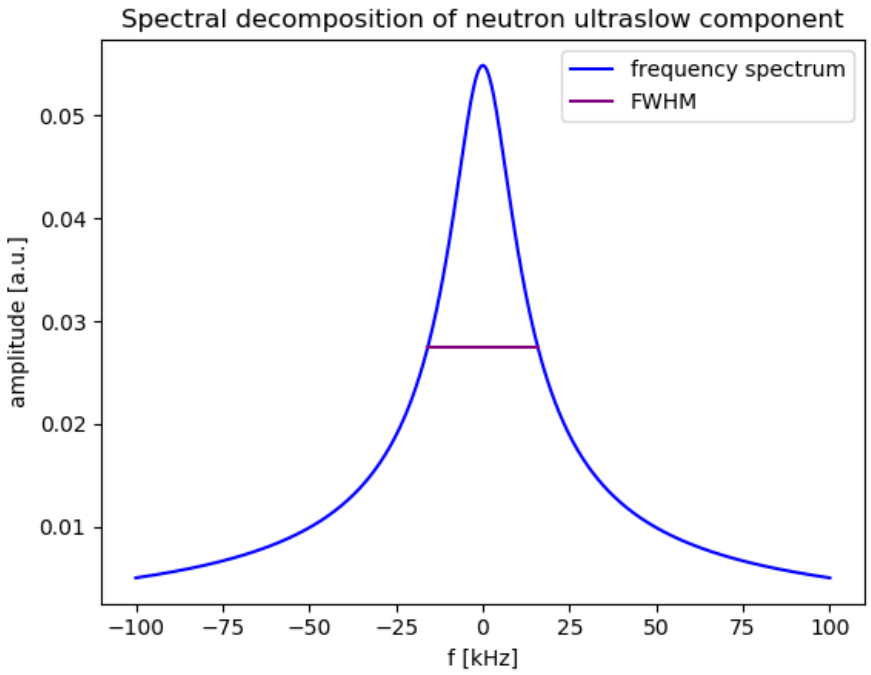

Figure 6.6: Spectral decomposition of neutron ultraslow component.

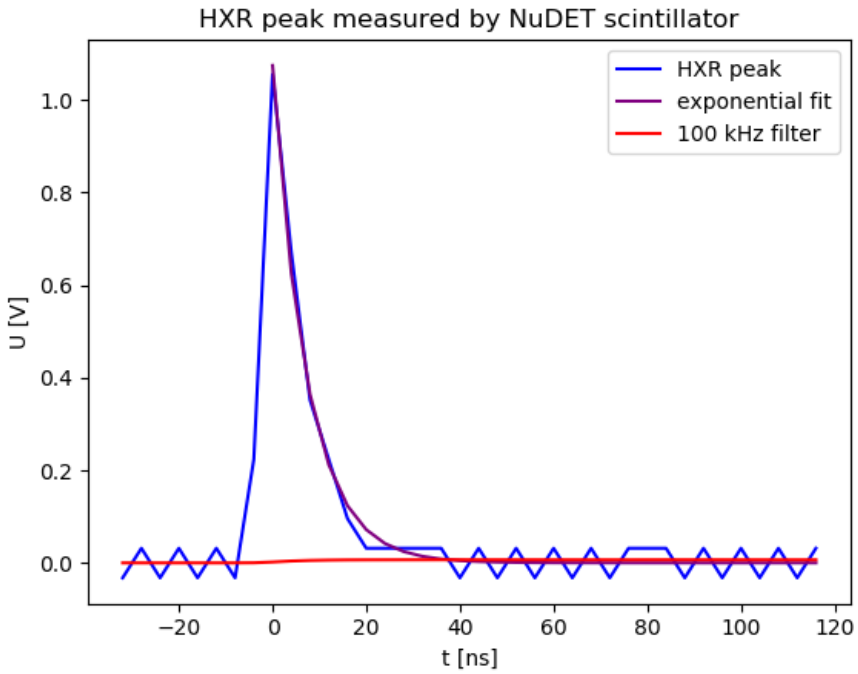

Figure 6.7: Application of 100 kHz lowpass bandwidth filter on HXR peak.

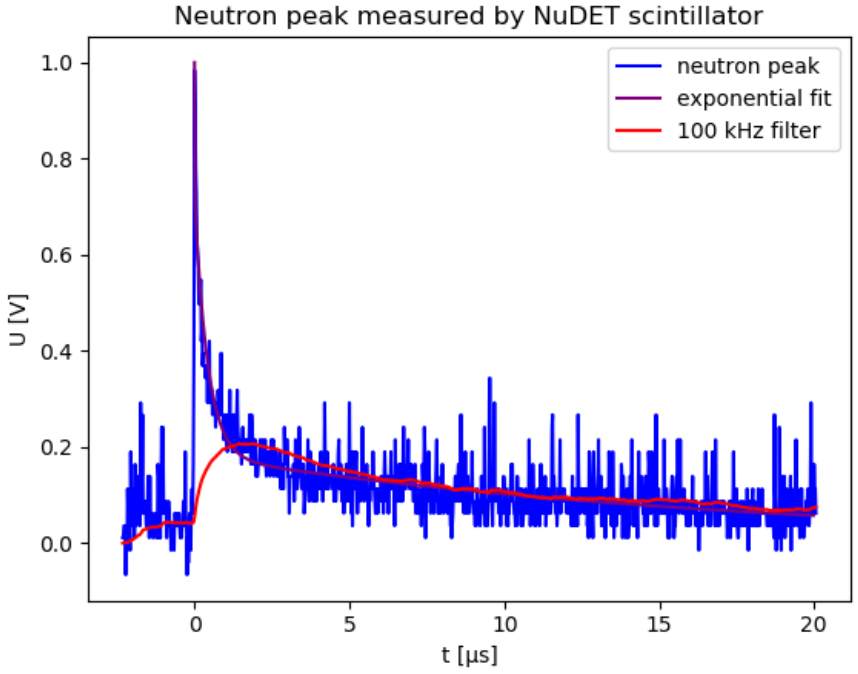

Figure 6.8: Application of 100 kHz lowpass bandwidth filter on neutron peak.

urally to a conclusion, that these neutrons are photo-neutrons raised from photo-disintegration reactions with the material of a tokamak compounds. The common sign of these discharges is the presence of Argon puff and also an additional big deuterium gas puff during discharge, but by a more detailed analysis of more campaigns together in the next section, we will clearly see, that deuterium gas puff is not the reason of high neutron counts.

The measurement of photo-neutrons from various photodisintegration reactions was also realised on the JET tokamak, see [6]. For more detailed informations about photo-neutron sources, see the chapter 5.5 or [31, 32].

DISCHARGE	HXRS	NEUTRONS
19984	57776	35
19985	504075	71
19990	1095793	146
19991	852639	136
20005	1007070	95

Table 6.2: The list of discharges with high neutron fluxes.

6.4.3 Time evolution of NuDET signal

Assuming that these neutrons are truly photo-neutrons, we should see visible correlation with high energy HXR flux time evolution. For this purpose we can use one of the photomultipliers without any crystals that are normally used to detect e.g. visible range bremsstrahlung radiation, but are also affected by HXRs in case of huge fluxes.

The figure 6.9 compares NuDET signal with HXR signal (photomultiplier tube) in representative discharge #19985 with high neutron fluxes. We can also see time histograms of detected HXR a neutron peaks. Resolution of neutron time histogram is quite low, because of only approx 70 neutron counts detected in the whole discharge. But we can still see, that a time evolution of neutron fluxes correlates to HXR time evolution, which clearly confirms, that these measured neutrons are photo-neutrons generated by the collision of REs with plasma facing components.

Photo-neutrons could be theoretically generated also by photo-disintegration reaction with deuterium in the plasma, but due to a many orders of magnitude lower concentration of a deuterium plasma ($\sim$ 1e19 m^{-3}) than the solid first wall components ($\sim$ 1e28 m^{-3}) it can be neglected.

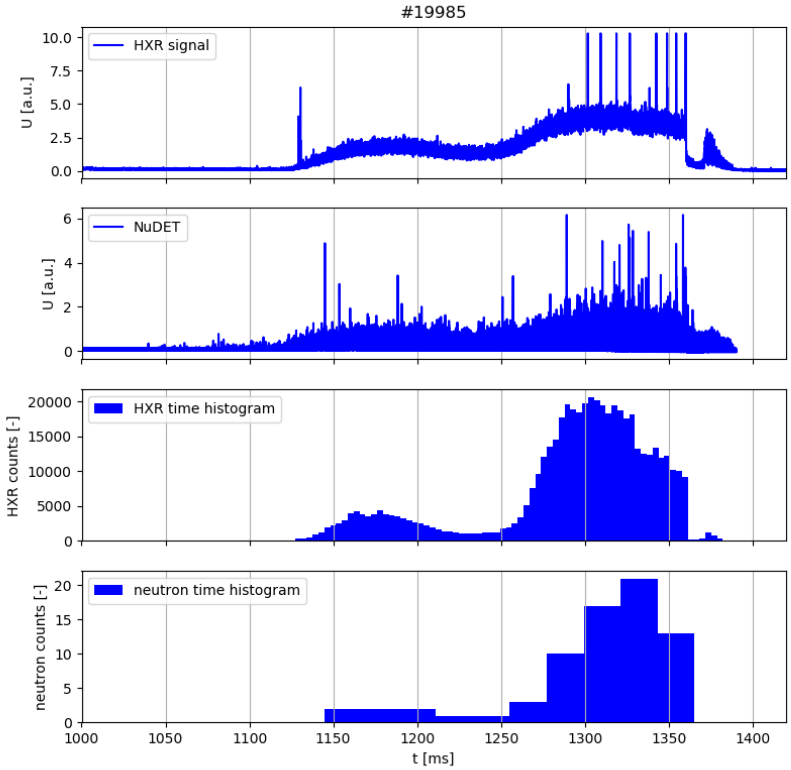

Figure 6.9: NuDET time histogram of the discharge #19985 in correlation with the HXR signal.

Chapter 7

Statistical analysis of photo-neutrons in RE campaigns

7.1 Basic overview

In chapter 3, we have analysed all the data from NBI campaigns and revealed the most important influences on fusion neutron gains. In this chapter, we will present similar analysis but with all useful data from neutron detectors in RE campaigns, thus we will statistically compare photo-neutron yields.

During the whole COMPASS tokamak operational period twelve RE campaigns took place. For the measurement of photo-neutrons, we can not use neutron detector EJ410, because we can not separate neutrons from HXR background. It should be possible, but with different data acquisition system. On the other hand, NuDET detectors were operational just in a few cases, like it was presented in the previous chapter or in chapter 4. Thus in this chapter, we will focus on 3He detectors Chadwick and Oliphant. Their big advantage is, that there is no necessary treatment of acquired data like in NuDET neutron/HXR separation, because the sensitivity of these detectors to HXR radiation is very marginal.

In the figure 7.1, we can see all neutron data from 3He detectors Chadwick and Oliphant. Both 3He detectors were added to COMPASS diagnostics later, so we can see "only" last seven RE campaigns. The whole 3He RE database contains a set of more than 500 discharges. But, as we can see in the figure 7.1, only in a very small part of these discharges intensive neutron yield was measured. Because measurement of photo-neutrons is very tightly connected to REs itself, this small set of discharges of high photo-neutron yield also represents a set, where high energy RE beam was generated.

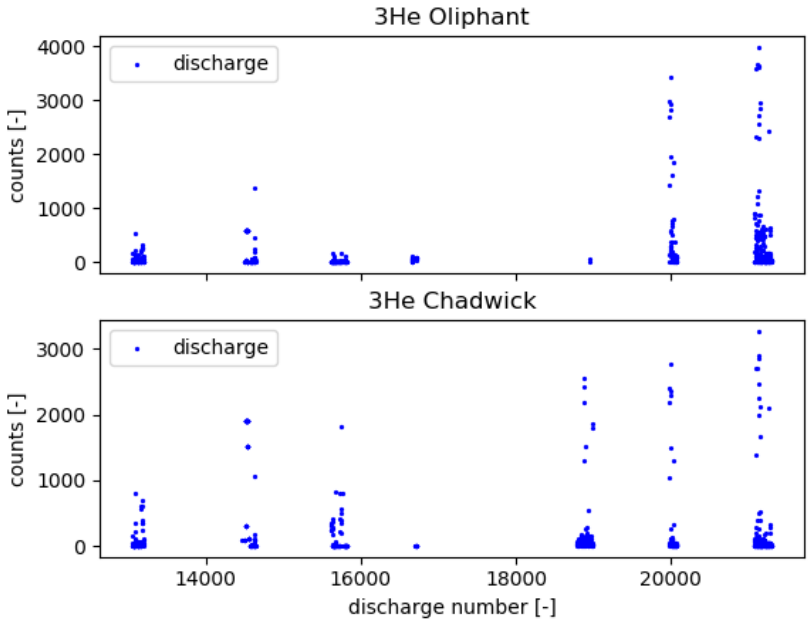

Figure 7.1: All neutron data from 3He detectors Oliphant and Chadwick from RE campaigns.

7.2 Filtering signals

In the analysis of NBI fusion neutrons, the expected neutron energy spectra should be very similar during all NBI campaigns. But here in RE campaigns, it is more complicated, because REs can in some discharges achieve probably just a low units of MeV or less (hundreds of keV), but on the other hand, the REs with the energy of 15 - 20 MeV are not quite excluded. Depending on which photo-nuclear reactions REs trigger and thus how much energy neutron will carry out as its kinetic energy, raised neutron energy spectra could be visibly different discharge from discharge. 3He detectors sensitivity is strongly dependent on its energy, so the comparison of neutron yields could be very tricky without eliminating this problem.

We can roughly eliminate this uncertainty in neutron energy spectra. Oliphant detector has HDPE moderator, which very roughly refine differences in Oliphant sensitivity for different neutron energies, as it moderates the fast neutrons. On the other hand, Chadwick has only lead shielding and the effect of this shielding on neutron energy spectra can be for simplicity neglected. In other words, a significant difference in neutron energy spectra should lead

to a different ratio of Oliphant vs Chadwick neutron counts.

Anyway, in this chapter, we have focused on discharges, where both 3He detectors were operational and also we have focused only on the discharges, where the Oliphant/Chadwick neutron ratio was in interval (1,2). It should ensure, that neutron energy spectra was reasonably similar and thus we can compare neutron yields between these discharges.

7.3 HXR flux dependence

Before analysis itself, it is good here to mention, that previously described database filtration based on Oliphant/Chadwick neutron ratio did not filtered out single one discharge with high photo-neutron fluxes. Thus, we can describe in the next rows the most dominant trends in photo-neutrons generation during RE campaigns.

Among many tokamak parameters and diagnostics output, the far most visible correlation in all data set is the one with the HXR signal (respectively integral of the HXR signal). This HXR diagnostics is a simple photomultiplier tube, which is naturally focused more on the broad visible and UV part. But in our situation (very high HXR fluxes), this diagnostics also measures HXR radiation. The photomultiplier tube was placed behind the shielding wall (the same place as NuDET detector was). An optical fiber from the plasma passes through the wall to this detector, but in RE campaigns, it is also disconnected in order to focus just on HXR radiation. This correlation is presented in the figure 7.2. We can see roughly a linear dependence. This correlation corresponds with previous results from NuDET detector.

In the figure 7.3, we can also see a correlation with the data from another HXR diagnostics, which is NaI(Tl) scintillation detector. If we focus on discharges with high neutron fluxes, we can also see roughly a linear trend, but the deviation is high. It can be explained by a susceptibility to saturation of the signal. Big NaI(Tl) crystal with very high sensitivity and a big electrical current yield from each registered photon is not suitable to such high HXR fluxes, which are present at tokamaks by RE beams. So, in our situation, the HXR signal from just a photomultiplier tube seems to be more reliable.

Based on the previously presented correlations, it is obvious, that these neutrons are photo-neutrons raised from photo-disintegration of tokamak structure atoms by HXR radiation released thanks to colliding runaway electrons. Thus in the next sections, we will use photo-neutron measurements to try to describe the basic behaviour of REs, reveal main trends.

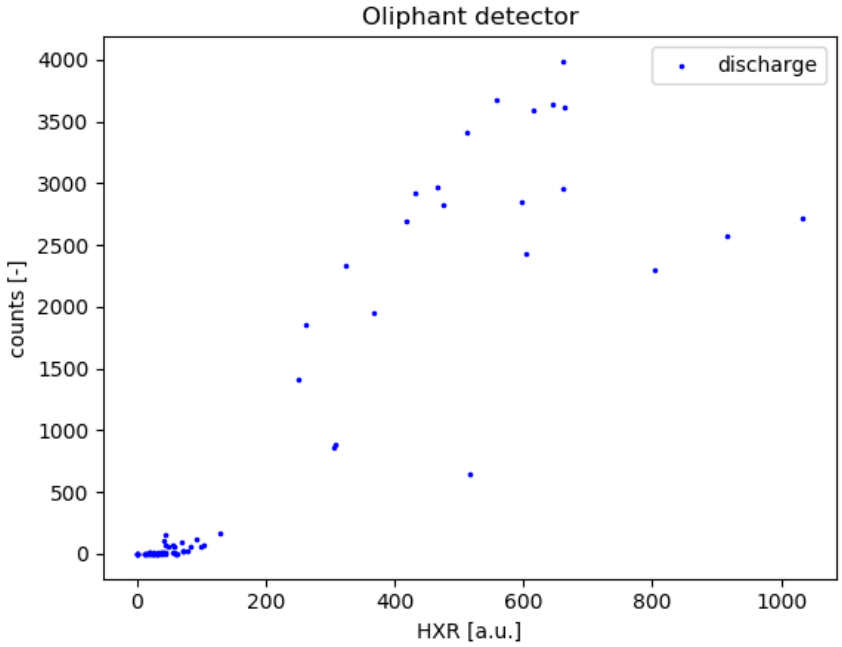

Figure 7.2: Correlation of photo-neutron counts with the integral of HXR signal from the photomultiplier tube.

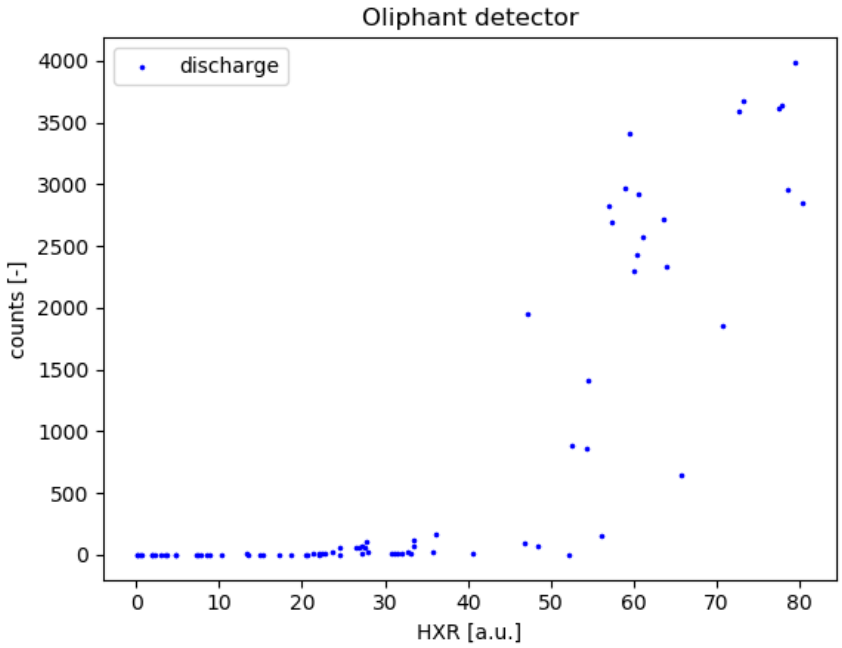

Figure 7.3: Correlation of photo-neutron counts with the integral of HXR signal from the NaI(Tl) detector.

7.4 Electric field dependence

Based on basic theory of REs, the very important influence on RE generation is the external electric field, which accelerates electrons to relativistic velocities. Here at the COMPASS tokamak, electrons are inductively driven by the current in central solenoid. The power source of this system of coils is called MFPS (Magnetizing Field Power Supply [33]). In the figure 8.2, there is shown the dependence of photo-neutron counts on the integral of MFPS current. Integral here represents well the heating attempt from central solenoid, because high derivation, which generates a loop voltage, leads naturally in our situation to higher integral also. It could be possible to take loop voltage directly, but it is very complicated to generally define good time interval for different RE discharges comparison. But MFPS current diagnostics is much more clearer and gives us approximately the same information.

Back to the figure 8.2, if we focus on discharges with high neutron counts (more than 500 counts), there is a visible linear dependence of photo-neutron counts on the MFPS current, which can be represented as the main accelerating electric field. This correlation corresponds well with RE theory.

But there are also discharges, where the MFPS current was intensive, but photo-neutrons were not measured at all or just very small values like the discharges marked by red color in the figure 8.2. It definitely seems connected with the argon puff, which its influence we will discuss in the next section.

7.5 Argon puff dependence

In the previous campaigns here at the COMPASS tokamak, it was confirmed the big argon puff in the ramp-up phase of discharges can invoke radiative disruption with current quench to generate REs. [25]

The one thing, which all discharges with high neutron counts have in common is the presence of Ar, Kr or Ne puff. On the other hand, none of red marked discharges with high MFPS current had this gas puff of high Z element. Ar or Kr gas puff was injected in all cases after the ramp-up phase. As a representative we use discharge #21132, in which we have measured the highest photo-neutron fluxes. The temporal evolution of the most interesting diagnostics is presented in the figure 7.5.

All presented diagnostics show a rise of activity approx 10 ms after argon gas puff (green color). It is obvious, that HXR (NaI(Tl)) and EJ410 diagnostics reach a saturation approx 100 ms after argon puff. HXR - photomultiplier tube diagnostics can handle these high fluxes and so the amplitude is gradually rising along with photo-neutrons detected with Oliphant detector (purple

color). The very first photo-neutrons are measured after a few ms after argon puff, but the truly intensive photo-neutron yield comes after approx 200 ms.

Argon causes generation of a RE beam, where the REs carry probably most of the measured current and are further accelerated. There is also a small current quench immediately after argon puff, which naturally boosts accelerating electric field in this short moment, thus in this moment a new (second) seed of REs can also arise. The first seed of REs is already present from ramp-up phase, as we can deduce from HXR signal (red).

In the time interval of approx. (1300,1400) ms, a rise of a photo-neutron yield is more intensive than a rise of HXR flux in the same interval. That clearly points out to probably a significant rise of RE energy, which is the influence of high acceleration by MFPS current.

In summary, an avalanche RE generation mechanism probably intensified the first seed and this phenomenon in a combination with the presence of the second RE seed and with intensive RE acceleration (high MFPS current) probably led to the most intensive RE beams and so the most intensive photo-neutron counts measured at the COMPASS tokamak. With the proviso that Argon puff had a very significant and more complex influence on this RE behaviour.

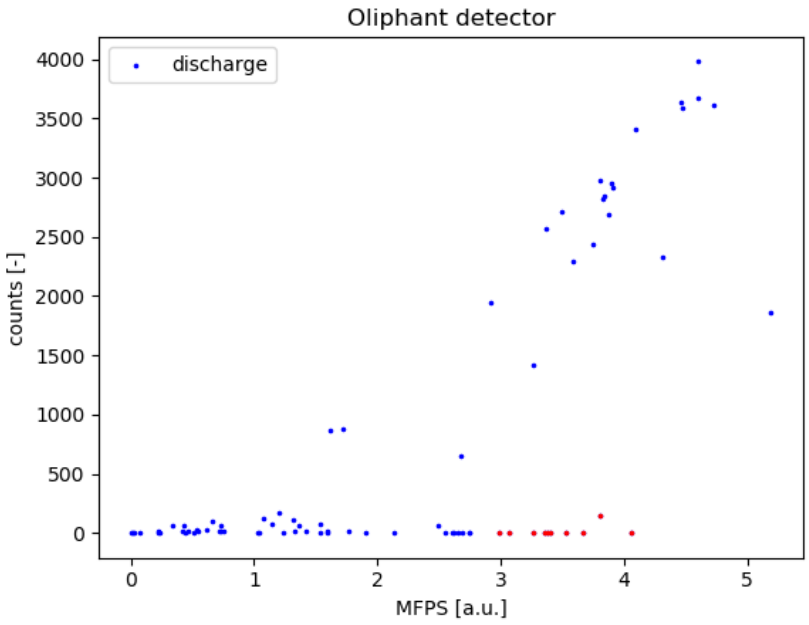

Figure 7.4: Neutron counts dependence on MFPS current.

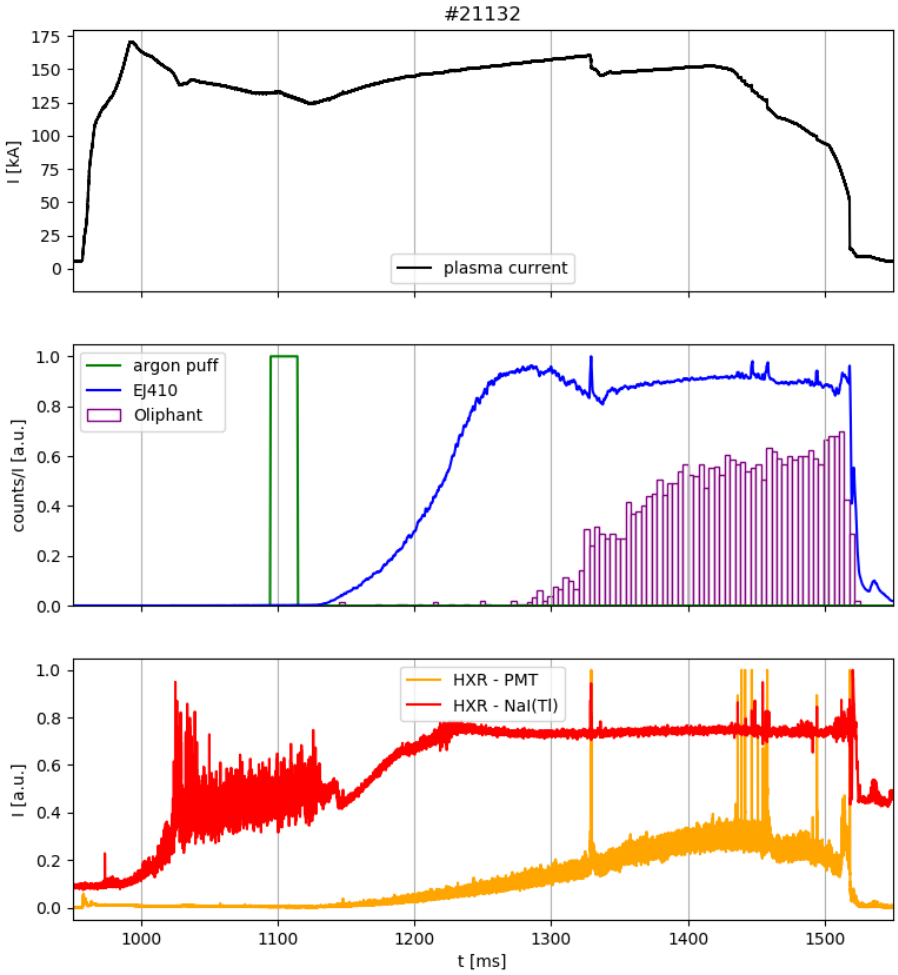

Figure 7.5: Temporal evolution of neutron and HXR diagnostics in the discharge #21132 with the most intensive photo-neutron yield.

Chapter 8

RE energy

8.1 Estimate of RE beam energy

In this section, we will present a very rough estimate of RE beam total energy based on the photo-neutron measurements. Our situation is, that REs generated in the plasma sooner or later collide with surrounding material a their energy is transferred into HXR radiation, which evokes photo-disintegration reactions, where the outcome are photo-neutrons measured in our detectors.

To achieve this, we need to take into account, that materials of plasma facing components have a quite wide range of photo-disintegration energy threshold. Figure 8.1 shows measured radioisotopes and corresponding (γ,n) reactions obtained by activation analysis at JET tokamak. This analysis was done, when JET used the same materials on plasma facing components as it is at COMPASS tokamak, thus divertor, HFS and limiters were protected by carbon tiles. It was observed, that RE beam did visible damage to the inconel (Ni-Cr austenitic alloy) vessel. Carbon tiles are on the other hand much more durable against RE damage. The same situation is at COMPASS tokamak: inconel vessel shielded by carbon tiles.

Carbon tiles can absorb complete RE beam, but the raised bremsstrahlung and especially its HXR part can definitely penetrate to the inconel vessel and surrounding tokamak structures. Due to obvious similarities of used materials, we can simply focus on the (γ, n) reactions presented in the figure 8.1.

Target	Reaction	Product	Threshold (MeV)	$T_{1/2}$	E_γ (keV)	%
^{12}C	γ, x(x=α+n)	^{7}Be	26.3	53.3 d	477.56	10.3
^{58}Ni	γ, p	^{57}Co	8.2	270.0 d	122.07	85.6
	γ, n	^{57}Ni	12.2	37.0 h	1377.62	84.9
	γ, np	^{56}Co	19.6	77.3 d	846.75	99.99
	γ, 2n	^{56}Ni	22.5	6.1 d	158.30	99.00
	γ, 2np	^{55}Co	29.5	18.0 h	931.50	75.00
^{62}Ni	γ, np	^{58}Co	20.0	70.8 d	810.75	99.45
^{54}Fe	γ, np	^{54}Mn	20.4	312.2 d	834.81	99.97
^{56}Fe	γ, np	^{52}Mn	20.9	5.7 d	1434.43	100.00
^{55}Mn	γ, n	^{54}Mn	10.2	312.2 d	834.81	99.97
^{52}Cr	γ, n	^{51}Cr	12.0	27.7 d	320.07	9.83
^{50}Cr	γ, np	^{48}V	21.6	15.97 d	983.50	100.0

Figure 8.1: List of studied nuclear reactions (column Reaction) based on detected radioisotopes (column Product) with its half-life (column $T_{1/2}$) by measurement of characteristic γ lines (column E_γ (keV)) at JET tokamak. [6]

8.1.1 Nickel photo-disintegration

To achieve an estimate of RE beam total energy as simply as possible, we come back to the data from the NuDET neutron detector, where detector measured behind the main shielding wall around the COMPASS tokamak. Here we can use a few simple assumptions in our calculation.

The main assumptions for this estimate are as follows:

- 1. Tokamak is like a spherical isotropic source of photo-neutrons. This assumption is to simplify the calculation. In fact, we do not have necessary informations for more accurate model, but our detectors measure in a horizontal direction, which should be the most intensive.
- 2. HXR photon collides with inconel chamber through the reaction

$$^{58}\mathrm{Ni}(\gamma, \mathrm{n})^{57}\mathrm{Ni}, \tag{8.1}$$

because the energy threshold of 12.2 MeV is almost the smallest one in the presented list in 8.1. Just a reaction with 52Cr has a little bit lower energy threshold of 12 MeV, but inconel alloy has much more Ni atoms than Cr.
- 3. We consider the REs are just a few MeV over an energy threshold and thus the cross-section of photo-disintegration reaction σ is approx. 10 mb for 15 MeV energy photons, based on cross-section in [34].
- 4. All photo-neutrons are thermalized ($E = 0.025$ eV) behind the wall. This leads to assume the maximal cross section of the reaction $^{6}\mathrm{Li}(\mathrm{n}, \alpha)\mathrm{T}$ in the NuDET detector.
- 5. We consider the case with the highest measured photo-neutron flux

(in NuDET database) - discharge #19990 with Argon puff, where we have measured 146 photo-neutron counts behind the shielding wall.

By using the assumptions 1. and 4. N_n was calculated as

$$N_n = 2,4 \cdot 10^{10}, \tag{8.2}$$

where N_n is the estimation of total number of photo-neutrons released in this discharge. We have used neutron wall attenuation coefficient equal to 84, estimated in the chapter 4 and the detector dimensional data and sensitivity presented in section 2.3. N_n is similar to generally considered numbers of total neutron outputs in NBI campaigns. If we consider, that we measure quite similar neutron counts in NBI discharges as in this discharge, then this estimate of N_n seems very solid.

The number of HXRs was simply calculated by using a thick target approximation, equation 5.2. Here, the number of reactions was N_n, the cross section was taken from the assumption 3. Here, we have considered the last rough approximation, that the HXR flux hits the target, which is a cube with a 5 cm thickness made from Ni (2. assumption). We need to approximate a target like this due to a definition of a thick target. This is however quite a deviation from the actual vessel wall thickness, that is just 4 mm. On the other hand the HXRs may hit surface almost tangentially, so these 5 cm of theoretical thickness of the Ni target could be reasonable.

The result is, that such "mono-energetic RE beam" of each photon energy of 15 MeV colliding dominantly with inconel vacuum vessel should contain total energy of 28,8 J. Based on diamagnetic diagnostics we know, that plasma should have about 3 kJ energy in this discharge (#19990). Because of the fact, that REs in plasma should gain a significant part of plasma energy, this estimate does not seem to be realistic.

Anyway, it needs to be mentioned, that this was very rough estimate due to a lack of many important precise informations. Some of presented assumptions can be in real wrong.

8.1.2 Carbon photo-disintegration

In the previous estimation of RE energy, we have simply chosen the most probable reaction of the presented list based on similar measurements at JET tokamak. But probably more interesting reaction is

$$^{13}\mathrm{C(p,n)}^{12}\mathrm{C}. \tag{8.3}$$

This photo-disintegration reaction has a lower energy threshold $E_\gamma \cong 5$ MeV. This reaction was not mentioned in the previous list in JET, because it produces stable isotope 12C, thus a contribution of this reaction can not be

measured by activation analysis.

We do not have a detailed information about carbon shielding tiles composition. So, based on [35], 13C stable isotope can have a very low concentration in natural graphite, but its concentration can be enhanced as well. Suppose, that carbon shielding tiles are compound of 10 % by 13C isotope (mass density of approx. 0.223 g/cm^3) and a cross-section of approx. 0.5 mb of 7 MeV HXR photons, figure [36]. Other assumptions are the same as in the previous section with Ni.

The result is, that such RE beam with this very specific conditions should contain the energy of 527 J. Assuming, that REs in this kind of discharges take over majority of the plasma current, this approximation of "mono-energetic RE beam" of 7 MeV interacting dominantly with the carbon shielding tiles corresponds much better with diamagnetic diagnostics (plasma energy of approx. 3 kJ) than the previous estimate of "mono-energetic RE beam" of 15 MeV interacting dominantly with inconel vacuum vessel. Another fact is, that majority of REs collides with the carbon shielding tiles, where the HXR density is thus the highest.

8.1.3 Deuterium photo-disintegration

As was already mentioned in section 6.4.3, there is also an option, that some photo-neutrons came from photo-disintegration reaction with deuterium nuclei in plasma. From the previous two estimates, it seems that energies of REs are rather around 7 MeV than 15 MeV definitely.

The energy threshold for deuterium photo-disintegration is 2.2 MeV ([28]), which is even less than with 13C. On the other hand, a concentration of deuterium plasma is approx. nine orders of magnitude lower than solid inconel or carbon tiles, so the contribution of deuterium gas photo-disintegration should be marginal.

The result is, that such RE beam interacting dominantly with deuterium plasma instead of plasma facing components should have a total energy of approx. 1 GJ energy, which is obviously a nonsense. Thus a contribution of deuterium photo-disintegration to photo-neutrons generation should be absolutely marginal.

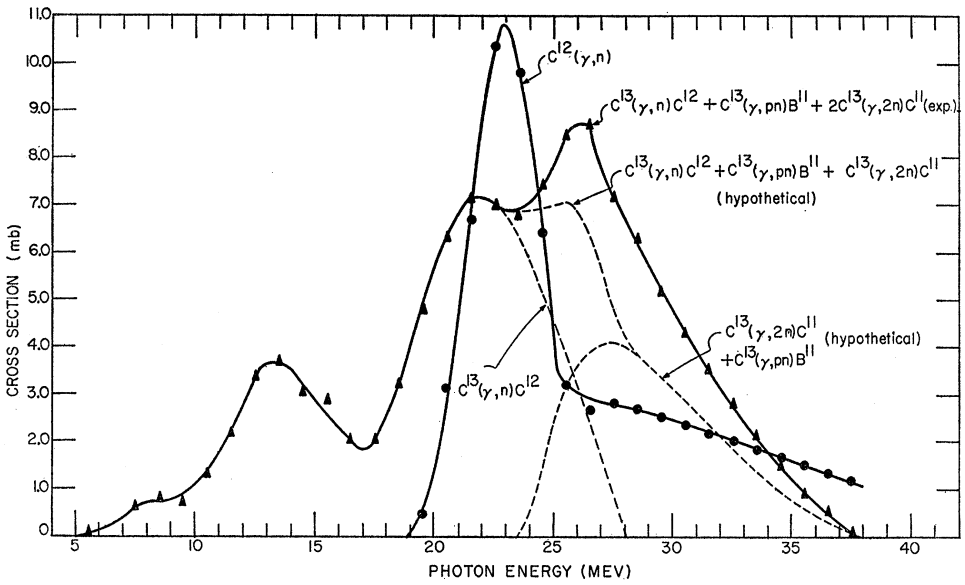

Figure 8.2: Cross-section of $^{13}\mathrm{C}(\mathrm{p},\mathrm{n})^{12\mathrm{C}}$. [36]

Conclusion

Statistical analysis of fusion neutron signals during the whole tokamak COMPASS standard operational period (2013-2020) revealed two significant trends in the data. First, that injected energy of NBI heating systems is absolutely crucial to gain a measurable fusion neutron yield here at the COMPASS tokamak. This correlation is so dominant, that it is visible even when all the neutron signal database is compared together, where many campaigns with different tokamak and plasma configurations were realised. The dependence of fusion neutron yield on NBI energy is closest to the linear dependence. This result can be considered as highly anticipated.

The second visible trend is, that plasma confinement mode significantly affects fusion neutron yield. If we compare discharges with the same NBI heating power, then triggering H-mode seems to lead to additional 25% of the neutron yield than in L-mode. It can be explained, that the rise of plasma temperature and plasma energy overcomes a worse NBI beam penetration to plasma due to a rise of plasma density in H-mode discharge. Anyway, it can be said, that H-mode leads to a rise of a confinement time of NBI fast ions and to a better fusion performance.

In the last chapter of the first part, we have demonstrated a specific measurement and a quite unconventional calculation of neutron wall attenuation coefficient. The result is, that the main shielding wall around the COMPASS tokamak should decrease the fusion neutron flux from the tokamak by roughly two orders of magnitude. This result is with a good correlation of theory and with the other measurement realised by another research group.

Very rough estimates of equivalent dose of neutron radiation were calculated both for COMPASS and COMPASS-U and the result is, that the equivalent dose behind the shielding wall should be many orders of magnitude lower than a set limit.

Statistical analysis of photo-neutron signals from RE campaigns revealed a

few significant trends in the data. First, that photo-neutron yield is clearly proportional to HXR radiation. This correlation is closest to the linear dependence. This result can be considered as highly anticipated and clearly confirms, that neutrons measured in RE campaigns are photo-neutrons raised from the collision of RE beam with the plasma facing components.

The second visible trend is, that a combination of Argon puff with high accelerating electric field leads to a very high photo-neutron yields, comparable to the amount of fusion neutrons realised in NBI campaigns. In the presence of Argon puff, the dependence of photo-neutron yield on the accelerating electric field from central solenoid seems to be linear. Anyway, it can not be said unequivocally, how precisely intensive RE beams in these specific discharges were generated. It seems to be much more complex process, which we can not deduce from our measured data.

Special measurement of REs behind the main shielding wall led to detailed analysis of NuDET scintillation detector signal, where the photo-neutron signals and the HXR signals were successfully identified and separated by use of 100 kHz low-pass bandwidth filter.

Thanks to successful neutron/HXR separation in NuDET detector, we have calculated a three rough approximations of RE beam like a mono-energetic RE beam reacting with specific material (nickel, carbon and deuterium) and we estimated its energy. The result is, that the approximation of mono-energetic RE beam with particle energy of 7 MeV interacting dominantly with carbon shielding tiles should contain the energy of 527 J, which is not so far from the information from diamagnetic diagnostics of 3 kJ stored in plasma energy in tested discharge. It could be explained, that many REs had energies lower than 5 MeV (energy threshold for 13C) and so its energy could not be transferred to photo-neutrons.

The calculation considering the nickel leads to a conclusion, that just a very small part of the RE beam could have an electron energy about 15 MeV. Approximation with deuterium as a target leads to a conclusion, that the contribution to photo-neutron yield raised from deuterium photo-disintegration should be absolutely marginal.

Bibliography

[1] K. Bogar, J. Stockel, J. Varju, and V. Weinzettl, "Energy composition of high-energy neutral beams on the COMPASS tokamak," *Nukleonika*, vol. 61, 12 2016.

[2] R. Panek, J. Adamek, M. Aftanas, P. Bilkova, P. Böhm, F. Brochard, P. Cahyna, J. Cavalier, R. Dejarnac, M. Dimitrova, O. Grover, J. Harrison, P. Háček, J. Havlíček, A. Havránek, J. Horacek, M. Hron, M. Imrisek, F. Janky, and J. Zajac, "Status of the COMPASS tokamak and characterization of the first H-mode," *Plasma Physics and Controlled Fusion*, vol. 58, p. 014015, 01 2016.

[3] M. Pickrell, A. Lavietes, V. Gavron, D. Henzlova, M. Joyce, R. Kouzes, and H. Menlove, "The iaea workshop on requirements and potential technologies for replacement of 3he detectors in iaea safeguards applications," *JNMM, Journal of the Institute of Nuclear Materials Management*, vol. 41, pp. 14–29, 03 2013.

[4] F. A. R. Schmidt, "THE ATTENUATION PROPERTIES OF CONCRETE FOR SHIELDING OF NEUTRONS OF ENERGY LESS THAN 15 MeV," tech. rep., OAK RIDGE NATIONAL LABORATORY, 1970.

[5] O. Ficker, "Generation, losses and detection of runaway electrons in tokamaks," Master's thesis, FJFI CVUT, 2015.

[6] O. Jarvis, G. Sadler, and J. Thompson, "Photoneutron production accompanying plasma disruptions in JET," *Nuclear Fusion*, vol. 28, p. 1981, 01 2011.

[7] https://www.iter.org/, 2022.

[8] F. Chen, *Úvod do fyziky plazmatu.* Academia, 1984.

[9] G. McCracken and P. Stott, *Fúze - Energie vesmíru.* Mladá fronta, 2006.

[10] R. Hemsworth, J. Feist, M. Hanada, B. Heinemann, T. Inoue, E. Küssel, V. Kulygin, A. Krylov, P. Lotte, K. Miyamoto, N. Miyamoto, D. Murdoch, A. Nagase, Y. Ohara, Y. Okumura, J. Paméla, A. Panasenkov, K. Shibata, M. Tanii, and M. Watson, "Design of the ITER Neutral Beam injectors," *AIP Conference Proceedings*, vol. 380, pp. 504–517, 07 1996.

[11] R. Panek, O. Bilyková, V. Fuchs, M. Hron, P. Chraska, P. Pavlo, J. Stockel, J. Urban, V. Weinzettl, J. Zajac, and F. Žáček, "Reinstallation of the COMPASS-D tokamak in IPP ASCR," *Czechoslovak Journal of Physics*, vol. 56, pp. B125–B137, 10 2006.

[12] J. Urban, V. Fuchs, R. Panek, J. Preinhaelter, J. Stockel, F. Zacek, V. Davydenko, and V. Mishagin, "NBI system for reinstalled COMPASS-D tokamak," *Czechoslovak Journal of Physics*, vol. 56, pp. B176–B181, 10 2006.

[13] F. Wagner, G. Becker, K. Behringer, D. Campbell, A. Eberhagen, W. Engelhardt, G. Fußmann, O. Gehre, J. Gernhardt, G. Gierke, G. Haas, and M. Huang, "Regime of Improved Confinement and High Beta in Neutral-Beam-Heated Divertor Discharges of the ASDEX Tokamak," *Physical Review Letters - PHYS REV LETT*, vol. 49, pp. 1408–1412, 11 1982.

[14] M. Bernert, *Analysis of the H-mode density limit in the ASDEX Upgrade tokamak using bolometry.* PhD thesis, Ludwig-Maximilians-Universität München, 2013.

[15] Y. Martin and T. Takizuka, "Power requirement for accessing the h-mode in ITER," *Journal of Physics: Conference Series*, vol. 123, p. 012033, 08 2008.

[16] D. Hill, "A review of ELMs in divertor tokamaks," *Journal of Nuclear Materials*, 1997.

[17] W. Muhammad, A. Hussain, and M. Maqbool, *Basic Concepts in Radiation Dosimetry*, pp. 9–41. 11 2017.

[18] L. Lobko, "Měření neutronů na tokamaku COMPASS." Bachelor thesis, 2019.

[19] K. Kirov, E. Belonohy, C. Challis, J. Eriksson, D. Frigione, L. Garzotti, L. Giacomelli, J. Hobirk, A. Kappatou, D. Keeling, D. King, E. Lerche, P. Lomas, M. Nocente, C. Reux, F. Rimini, G. Sips, and D. Van Eester, "Analysis of the fusion performance, beam-target neutrons and synergistic effects of JET high performance pulses," *Nuclear Fusion*, vol. 61, 01 2021.

[20] O. Ficker, "Neutron measurements at COMPASS," 2019. Powerpointová prezentace.

[21] J. Mlynář, "Fúzní jaderné reakce," 2018. Přednáška a powerpointová prezentace k předmětu Úvod do termojaderné fúze na FJFI, ČVUT.

[22] V. Wagner, "Lectures from subject "Úvod do jaderné fyziky" at FNSPE CTU in Prague," 2018.

[23] H. Shatkay, "The fourier transform – a primer," 10 1996.

[24] C. Liu, *Runaway electrons in tokamaks*. PhD thesis, Princeton university, 2017.

[25] M. Farnik, J. Urban, J. Zajac, O. Bogar, O. Ficker, E. Macusova, J. Mlynar, J. Cerovsky, M. Varavin, V. Weinzettl, M. Hron, and the COMPASS team, "Runaway electron diagnostics for the COMPASS tokamak using EC emission," *45th EPS Conference on Plasma Physics*, 2018.

[26] S. Bozhenkov, M. Lehnen, K. Finken, M. Jakubowski, R. Wolf, R. Jaspers, M. Kantor, O. Marchuk, E. Uzgel, G. Van Wassenhove, O. Zimmermann, D. Reiter, and t. team, "Generation and suppression of runaway electrons in disruption mitigation experiments in TEXTOR," *Plasma Physics and Controlled Fusion*, vol. 50, p. 105007, 08 2008.

[27] O. Ficker, E. Macusova, J. Mlynář, D. Bren, A. Casolari, J. Cerovsky, M. Farník, O. Grover, J. Havlicek, A. Havranek, M. Hron, M. Imrisek, M. Jerab, J. Krbec, P. Kulhanek, V. Linhart, M. Marcisovsky, T. Markovic, D. Naydenkova, and C. Reux, "Runaway electron beam stability and decay in compass," *Nuclear Fusion*, vol. 59, 05 2019.

[28] R. Schiavilla, "Induced polarization in the $^2\mathrm{H}(\gamma, \vec{n})^1\mathrm{H}$ reaction at low energy," *Phys. Rev. C*, vol. 72, p. 034001, Sep 2005.

[29] F. E. Myers and L. C. Van Atta, "On the Photodisintegration of Beryllium and Deuterium," *Physical Review*, 1942.

[30] F. Pino, L. Stevanato, D. Cester, G. Nebbia, L. Sajó-Bohus, and G. Viesti, "Study of the thermal neutron detector ZnS(Ag)/LiF response using digital pulse processing," *Journal of Instrumentation*, vol. 10, pp. T08005–T08005, 08 2015.

[31] A. Wattenberg, "Photo-neutron sources and the energy of the photoneutrons," *Phys. Rev.*, vol. 71, pp. 497–507, Apr 1947.

[32] D. Salehi, M. Jozani, and D. Sardari, "Characteristics of a heavy water photoneutron source in boron neutron capture therapy," *Chinese Physics C*, vol. 37, 07 2013.

[33] J. Havlicek, J. Horacek, V. Weinzettl, O. Hronova, D. Naydenkova, and J. Zajac, "Magnetic diagnostics for start-up phase of COMPASS," *WDS'09 Proceedings of Contributed Papers: Part II - Physics of Plasmas and Ionized Media*, 01 2009.

[34] H. Utsunomiya, T. Renstrøm, G. Tveten, S. Goriely, S. Katayama, T. Arizumi, D. Takenaka, D. Symochko, B. Kheswa, V. W. Ingberg, T. Glodariu, Y.-W. Lui, S. Miyamoto, A. C. Larsen, J. Midtbø, A. Görgen, S. Siem, L. Crespo Campo, M. Guttormsen, and A. Koning, "Photoneutron cross sections for Ni isotopes: Toward understanding (n, γ) cross sections relevant to the weak s-process nucleosynthesis," *Physical Review C*, vol. 98, 04 2018.

[35] https://en.wikipedia.org/, 2022.

[36] B. C. Cook, "Photodisintegration of C13," *Physical Review*, 1957.